Low-Cost Visual/Inertial Hybrid Motion Capture System for Wireless 3D Controllers

by

Alexander Wong

A thesis

presented to the University of Waterloo

in fulfilment of the

thesis requirement for the degree of

Master of Applied Science

in

Electrical and Computer Engineering

Waterloo, Ontario, Canada, 2007

I hereby declare that I am the sole author of this thesis. This is a true copy of the thesis, including any required final revisions, as accepted by my examiners.

I understand that my thesis may be made electronically available to the public.

Abstract

It is my thesis that a cost-effective motion capture system for wireless 3D controllers can be developed through the use of low-cost inertial measurement devices and camera systems. Current optical motion capture systems require a number of expensive high-speed cameras. The use of such systems is impractical for many applications due to its high cost. This is particularly true for consumer-level wireless 3D controllers. More importantly, optical systems are capable of directly tracking an object with only three degrees of freedom. The proposed system attempts to solve these issues by combining a low-cost camera system with low-cost micromachined inertial measurement devices such as accelerometers and gyro sensors to provide accurate motion tracking with a full six degrees of freedom. The proposed system combines the data collected from the various sensors in the system to obtain position information about the wireless 3D controller with 6 degrees of freedom. The system utilizes a number of calibration, error correction, and sensor fusion techniques to accomplish this task. The key advantage of the proposed system is that it combines the high long-term accuracy and low frequency nature of the camera system and complements it with the low long-term accuracy and high frequency nature of the inertial measurement devices to produce a system with a high level of long-term accuracy with detailed high frequency information about the motion of the wireless 3D controller.

Acknowledgements

First, let me start by thanking God for giving me strength in my research. Secondly, I wish to thank my supervisors Professor William Bishop and Wayne Loucks. In particular, I with to thank Professor William Bishop for his advice and moral support throughout my time under his supervision. He has contributed tremendously to my growth as a dedicated researcher.

I wish to thank all of the funding agencies and corporations that supported my research through financial and knowledge support. In particular, I wish to thank Epson Canada Ltd., and the Natural Sciences and Engineering Research Council (NSERC) of Canada. I wish to especially thank Ian Clarke and Hui Zhou for making the collaboration with Epson Canada Ltd. possible as well as invigorating my love for research.

Finally, I wish to thank my family (especially my mother Rosemary and my sister Scarlett), my friends and the colleagues at both University of Waterloo and Epson Canada Ltd. for their unconditional support.

Contents

1 Introduction **1**

1.1 Motivation 2

1.2 Statement of Thesis 4

1.3 Outline of the Thesis 6

2 Background **7**

2.1 Magnetic Motion Capture Systems 7

2.2 Mechanical Motion Capture Systems 8

2.3 Optical Motion Capture Systems 10

2.4 Inertial Motion Capture Systems 11

2.5 Hybrid Motion Capture Systems 13

3 Motion Capture System **14**

3.1 Introduction 14

3.2 Structural Overview 16

3.2.1 Hardware 16

3.2.2 Software 19

4 Inertial Measurement Unit (IMU) **22**

4.1 Introduction 23

4.2 Background Theory 25

4.3 IMU Structural Overview 27
4.4 Sources of Error and Error Model 29
4.5 Rate Gyro Error Evaluation 32
4.5.1 Experimental Results 34
4.6 Accelerometer Error Evaluation 36
4.6.1 Experimental Results 37

5 Inertial Navigation Unit (INU) 40
5.1 Introduction 41
5.2 INU Structural Overview 42
5.3 Angular Velocity Processing Unit 43
5.3.1 Frame of Reference Calibration 43
5.3.2 Data Integration and Error Reduction 45
5.4 Acceleration Processing Unit 46
5.4.1 Error Reduction 47
5.4.2 Frame of Reference Transformation 47
5.4.3 Data Integration 52

6 Visual Tracking Unit (VTU) 54
6.1 Introduction 54
6.2 VTU Structural Overview 56
6.3 Object Detection 56
6.4 Position Estimation 64
6.5 Experimental Results 67

7 Vision-Inertial Fusion Unit (VIFU) 69
7.1 Introduction 69
7.2 Sensor Fusion Techniques 72
7.2.1 Complementary Filters 72

7.2.2 Kalman Filters 73
7.3 VIFU Structural Overview 76
7.4 Error-State Complementary Kalman Filter 76

8 Conclusions **82**
8.1 Thesis Contributions 83
8.2 Potential for Future Research 84
8.2.1 Low-Cost Multi-Marker Visual-Inertial Motion Capture . . . 84
8.2.2 Mainstream Software Applications Utilizing Motion Capture 85
8.3 Thesis Applicability 85

Bibliography **86**

List of Tables

2.1 Comparison of existing motion capture techniques 13

4.1 Summary of orientation accuracy tests 34
4.2 Summary of position accuracy tests 37

6.1 Specifications of the test camera system 68
6.2 Summary of VTU position accuracy test 68

7.1 Summary of position accuracy tests 80

List of Figures

3.1 Hardware setup of the proposed motion capture system 18
3.2 Setup of the wireless 3D controller 19
3.3 Overall software architecture of the proposed motion capture system 20

4.1 Operation of a piezoelectric-based vibrating gryo sensor 24
4.2 3D tri-axis coordinate system 25
4.3 3D orientation as represented using Euler angles 26
4.4 Device frame of reference 28
4.5 Camera frame of reference 28
4.6 Sample test trial from position accuracy tests 39

5.1 INU setup 42
5.2 Sample calibration alignment 44
5.3 Effect of constant bias removal 48
5.4 Frame of reference transform 50

6.1 VTU setup 56
6.2 A cylindrical visualization of the HSV colour 58
6.3 Initial colour thresholding of video frame 60
6.4 Classic Hough transform of a line 61
6.5 Circular Hough transform of a point 63
6.6 Results of object detection 65

6.7 Inverted pinhole camera model 66

7.1 Complementary filter system 73
7.2 VIFU setup 77
7.3 Error-state complementary Kalman filter 78
7.4 Position error over time for error-state complementary Kalman filter 81

Chapter 1

Introduction

This dissertation presents the design of a low-cost motion capture system using both optical sensors and inertial sensors. Previous research has demonstrated the effectiveness of such multi-sensor hybrid systems. The goal of this research is to investigate and analyze the issues related to the design of such hybrid systems for the purpose of tracking wireless input devices such as pen-based controllers. Such a system provides a higher level of interactivity and control with respect to absolute position and orientation of the 3D controller. This dissertation provides practical solutions to the issues involved in the development of the proposed system such as error reduction and correction, managing different frames of reference, and sensor data fusion.

1.1 Motivation

Motion capture (or motion tracking) is the process of recording the movements of an object. Motion capture systems are widely used in many diverse fields such as:

Animation – Motion capture systems have been used to capture the movements of humans and animals to both enhance the realism of computer animated characters in movies and video games. The other main benefit of motion capture for use in movies and video games is that it can reduce the cost of animation by eliminating the need for individual frames to be drawn by hand.

Medical – Motion capture systems have also been used in the medical field for a number of different applications. One such application is the early diagnosis of movement-related disorders such as Parkinson's disease [YAG+03] and Multiple Sclerosis. Another application in the medical field is in biomechanical research, where motion capture devices allow medical scientists to study the mechanics of human motion to get a better understanding of how motion behaviour relates to disease formation.

Simulation/Augmented Reality – Motion capture systems have also been used to improve the realism of simulations and other augmented reality applications. By capturing the movement of the user, it is possible to dynamically adapt the simulation to reflect the user's actions. For example, wearable motion capture devices have been designed to track head movement. This allows a simulation to change what is displayed on a display based on the direction the user is looking.

Sports – Motion capture systems have primarily been used in sports for the pur-

pose of motion analysis. The motion of an athlete is recorded while he or she is performing an action, such as hitting a ball or performing a jump. This motion data is then analyzed to suggest changes to the way the athlete moves to improve his or her efficiency and performance.

Entertainment – Motion capture systems have recently made their way into the area of interactive entertainment. New video game input devices have been designed by Nintendo Inc. and Sony Computer Entertainment Inc. to allow the player to interact with the game environment at a higher level of immersion. These systems include the camera-based EyeToy® [Eye06] from Sony and the inertial-based Wii® remote [Wii06] from Nintendo. Being a relatively new concept in the video game industry, such devices are mainly useful for basic control actions due to technological limitations.

Despite the wide range of applications that can take advantage of motion capture systems, such systems have been largely limited to being used in studio environments. This is mainly due to the fact that current commercial motion capture systems require expensive components such as multiple high-speed optical cameras. Another reason that motion capture systems have not been widely adopted in the consumer market is that current motion capture systems require controlled environments to function properly. Therefore, it is necessary to find low-cost alternatives to existing systems that can be used in less ideal situations.

One promising approach to robust motion capture is the development of multi-sensor hybrid systems. These systems take advantage of the strengths of different sensor modalities to achieve better accuracy and performance. Recent advances in sensor technology have made such an approach to motion capture economically feasible for low-end commercial applications such as the tracking of wireless input

devices. Advances in Micro-Electro-Mechanical Systems (MEMS) have lead to the development of miniature, low-cost inertial devices such as gyros and accelerometers. Furthermore, advances have also been made in Charged Coupled Device (CCD) manufacturing has lead to low-cost digital camera systems.

Low-cost inertial sensors such as gyros and accelerometers are capable of collecting accurate data over short periods of time at a high sample rate. However, error accumulates over time when the measurements captured by these devices are used to obtain displacement and orientation information. Therefore, systems that rely solely on low-cost inertial sensors are unable to maintain long-term accuracy. On the other hand, low-cost camera sensors are capable of providing accurate measurements over a long period of time. However, due to the amount of processing involved in extracting and interpreting information from visual data obtained from cameras, systems that rely solely on visual data can only operate at a low sample rate. Therefore, inertial and visual sensing can be viewed as complementary sensor technologies as each have different strengths that compensate for each other's weaknesses. As such, a system that combines both visual and inertial sensors has the potential to provide more robust and accurate motion capture capabilities than if they were used separately. Therefore, the main goal of the research presented by this dissertation is to develop a hybrid motion capture system using both inertial and visual sensors.

1.2 Statement of Thesis

It is my thesis that a hybrid vision-inertial approach to motion capture has the potential to provide superior tracking information of wireless 3D controllers when

compared to a system consisting of only vision sensors or inertial sensors. A hybrid system makes it possible for the use of low-cost off-the-shelf sensor components to provide accurate, detailed, and robust 3D motion tracking. Furthermore, such a system can operate reliably at a high resolution in non-ideal environments such as an office or a home. This in turn opens up the possibility for consumer-level, wireless 3D controllers that can provide absolute position and orientation in 3D space and thus allows for a greater level of interactivity.

The design of a vision-inertial system for low-cost 3D motion tracking of wireless 3D controllers poses a number of different challenges. These include measurement error reduction and prediction, coordinate system calibration, and data fusion. As such, the proposed system is broken into separate components, each dealing with a specific challenge. This modularization allows different sensors, filters, and processing units to be removed and added according to the needs of the specific device.

In some respects, the concept of the proposed system is similar to that proposed in [SYA99], where vision and inertial data are fused to provide improved motion tracking robustness and accuracy. However, the underlying goal is very different. The system proposed in [SYA99] utilizes the motion tracking information for the purpose of augmented reality registration and therefore focuses on tracking the environment to align it with a virtual environment based on the point of view of the user. Therefore, both the vision sensors and inertial sensors are centralized at the user. However, the goal of this thesis research is to utilize motion tracking information for the purpose of tracking a wireless 3D controller with respect to the environment. As such, the vision sensors and inertial sensors are decentralized in the proposed system to accommodate for object tracking.

1.3 Outline of the Thesis

Chapter 2 presents a background overview of existing motion capture systems. Chapter 3 presents an overview of the hardware and software architecture of the proposed motion capture system. Chapter 4 describes the inertial measurement unit (IMU) in detail. The sources of error associated with rate gyros and accelerometers used in the IMU are presented along with an error model for inertial sensors. Furthermore, experimental results from stationary and dynamic error evaluation tests are presented and analyzed in detail. Chapter 5 describes the design of the inertial navigation unit (INU) used to determine relative 3D position and orientation information from the raw data provided by the IMU. The error reduction techniques used in the INU and the corresponding test results are also presented. Chapter 6 describes the design of the visual tracking unit (VTU) used to determine absolute 3D position from the visual data acquired by the camera system. The marker detection and position estimation methods are described in detail. Chapter 7 describes the design of the vision-inertial fusion unit (VIFU) used to combine the information from the VTU and INU into 3D position information that is more detailed than that provided by the VTU and more accurate and robust than that provided by the INU. Chapter 8 discusses the thesis contributions and potential topics for future research.

Chapter 2

Background

A great deal of research has been conducted in the area of motion capture and tracking. While a large number of different sensor technologies have been used, motion capture and tracking technologies can be grouped into categories:

1. Magnetic,
2. Mechanical,
3. Optical, and
4. Inertial.

2.1 Magnetic Motion Capture Systems

In magnetic motion capture systems [Asc06, YAG+03, JOH00], magnetic sensors are placed on the object being tracked. These sensors measure the magnetic field

being generated by a magnetic transmitter. Based on these measurements, position and orientation information can be calculated with respect to the transmitter. One such system is the MotionStar magnetic motion capture system from Ascension Technology Corp. [Asc06], which has been used for tasks such as joint parameter estimation [JOH00]. There are a number of advantages to magnetic motion capture systems. First, such systems are not affected by occlusion as optical systems are. Furthermore, magnetic motion capture systems can measure absolute positioning of an object in 3D space. However, there are also a number of disadvantages to utilizing magnetic motion capture systems. First, the strength of magnetic fields decreases greatly as the distance from the transmitter increases. This effectively limits the motion capture area of such systems. Second, the data acquired through this technique is generally more noisy than that obtained using optical systems. Most importantly, magnetic motion capture systems are highly sensitive to magnetic interference, which may occur due to external wiring and/or multiple tracked objects in close range. This makes it poorly suited for consumer-level motion tracking, which must be capable of operating in non-ideal environments such as homes.

2.2 Mechanical Motion Capture Systems

In mechanical motion capture systems, a rigid exoskeleton that contains sensors at each joint is attached to the object being tracked (typically a person). When the object moves, the mechanical segments of the exoskeleton move along with the object. The motion of the mechanical segments is then recorded by the sensors at the joints to determine the relative motion of the object. An example of a mechanical motion capture system is the Gypsy5 motion capture system from An-

imazoo [Ani06], which consists of 37 potentiometers and 17 joints and is designed to be worn by a human for the purpose of motion capture. There are a number of advantages to mechanical motion capture systems. First, since the system captures relative motion at the joints, it is not affected by occlusion as optical systems are. Secondly, such systems can acquire data at a high sampling rate as the sensed data does not require a lot of processing to extract motion information. Finally, mechanical motion capture systems consist primarily of plastic or metal rods for segments and potentiometers for sensors. Therefore, these systems can be constructed at relatively low cost when compared to optical systems.

There are a number of disadvantages to mechanical motion capture systems. First, such systems are unable to directly measure the absolute positioning of an object. While absolute positioning may be inferred based on information about the original reference position, this imposes additional limitations on the range of actions performed by the object. For example, the performer using such as system is not allowed to jump if absolute positioning is required since the change in absolute positioning cannot be inferred from the relative motion measured by the system. Secondly, the need for an exoskeleton makes mechanical motion capture systems cumbersome when compared to other motion capture techniques. Finally, such systems are suitable only for objects with moveable joints such as human performers. Therefore, such techniques are not suitable for tracking the motion of rigid objects such as wireless 3D controllers.

2.3 Optical Motion Capture Systems

In optical motion capture systems, a number of markers are placed on the object being tracked. Optical cameras are then used to track the individual markers on the object. The captured visual information is then processed by the motion capture system and used to triangulate the 3D position of each individual marker. Optical systems can be grouped into two categories: i) Passive, and ii) Active. In passive optical systems such as those produced by Vicon [Vic06], retro-reflective markers are placed on the object being tracked and strobe lights are then used to illuminate the markers so that they can be tracked by the camera. The main advantage of passive systems over active systems is that the markers placed on the object being tracked does not contain any electronic equipment, thus allowing for more flexibility in certain situations. In active optical systems such as the OPTOTRAK systems from NDI [NDI06], the markers contain embedded emitters. For example, the PhaseSpace motion capture system [Pha06] can track up to 128 unique active LED markers. The main advantage of active systems over passive systems is that each marker can be uniquely identified. This allows for faster resolution of marker overlaps as well as reduce the processing time required to track and distinguish individual markers. As a result, active systems can perform at higher speeds than passive systems at the expense of increased cost and reduced convenience.

There are a number of advantages to the use of optical systems over other methods. First, optical motion capture systems can measure absolute positioning of an object in 3D space. Second, the data obtained using such systems are in general cleaner than other techniques. Optical systems are flexible in terms of placement on the object and therefore allows for greater freedom of motion. Furthermore, it allows for multiple objects to be tracked simultaneously. Despite all of these

benefits, there are some notable disadvantages to optical motion capture systems. First, optical systems are susceptible to the effects of marker occlusion. The effects of occlusion can be reduced through interpolation as well as the addition of cameras to reduce the probability of occlusion, but result in increased computational and/or economical costs. Another disadvantage of optical systems is that they are incapable of measuring 3D orientation in a direct manner. Orientation must be calculated indirectly based on the relative positioning between neighboring markers. Not only does this add to the computational cost of the system, it also makes it impossible to determine orientation on objects that contain a single marker. This makes the use of purely optical data ill-suited for tracking wireless 3D controllers which may be marked at a single location. Finally, optical motion capture systems require a greater amount of computational processing than other techniques due to the complexity of extracting information from visual data and then determining absolute positioning and orientation based on that information. This is particularly true for passive systems, where the software must also distinguish between different markers. As such, most passive systems cannot be operated in a real-time scenario. Therefore, it is difficult to implement an optical system based solely on low-cost cameras with a high level of detail in a real-world environment.

2.4 Inertial Motion Capture Systems

The final main category of motion capture systems are those based on inertial sensor devices. In inertial motion capture systems, inertial sensors such as gyros and accelerometers are used to measure the relative motion of the object being tracked. Gyros are used to determine orientation while accelerometers are used to determine

acceleration. By placing the sensors normal to each other, inertial motion capture systems can determine the relative 3D orientation and position at a particular point. Inertial motion capture systems have been used extensively for vehicle navigation and tracking [JLA95, DGEE03] and human motion tracking [Lui02, Roe06]. There are a number of advantages to the use of inertial motion capture systems. First, it provides direct measurement in 6 degrees of freedom (DOF), which cannot be achieved using an optical system. This makes it well suited for tracking both 3D position and orientation of rigid objects with a single sensor location, such as wireless 3D controllers. Second, it is capable of acquiring motion data at a high sampling rate, as well as requiring less processing power than optical systems. This allows it to provide very detailed motion information. Furthermore, it is not affected by visible occlusion. Finally, like optical systems the placement of sensors is flexible and allows for the object to perform a greater range of motions. There are two main disadvantages to inertial motion capture systems. First, like mechanical systems they are unable to directly measure the absolute positioning of an object. This imposes some limitations on the range of actions performed by the object. More importantly, inertial sensors does not measure position and orientation explicitly, but derives the information based on measured acceleration and angular velocity. This leads to rapid error accumulation over time and therefore are stable only in short periods of time. This makes error reduction and correction very crucial in the design of an accurate inertial motion capture system.

2.5 Hybrid Motion Capture Systems

More recent work on motion capture systems center around hybrid systems, which make use of different sensors to provide more robust and accurate 3D position and orientation measurements. These include systems based on a combination of acoustic and inertial [EFGP98], magnetic and vision [CJD03], GPS and inertial [SH05, Sch06], and inertial and vision [Blo06, FN03a, FN03b, KD04, RLG+02, SYA99]. A comparison of existing motion capture techniques is presented in Table 2.1.

Table 2.1: Comparison of existing motion capture techniques

Criteria	**Magnetic**	**Mechanical**	**Optical**		**Inertial**
			Passive	**Active**	
Cost	Med-High	Low	Med-High	High	Low
Complexity	High	Low-Med	High	Med-High	Low-High
Resolution	Low	High	Low-High	Low-High	High
Accuracy	Low-Med	High	High	High	High
Positioning	Absolute	Relative	Absolute	Absolute	Relative
Range	Low	N/A†	Low-Med	Low-Med	Med-High
Highly Susceptible to Occlusion	N	N	Y	Y	N

†Measures only relative motion, so range is not applicable.

Chapter 3

Motion Capture System

This chapter briefly describes the overall architecture of the proposed motion capture system. The first section presents an introduction to the problems and issues faced during the design of the system. Furthermore, the design philosophy behind the proposed system architecture is presented. The next section provides a structural overview of the system, both on a hardware and software level. First, the environment setup of the system is described in detail. Second, the placement of sensors in the actual wireless 3D controller is presented. Finally, the architectural overview of the underlying software processing system is described.

3.1 Introduction

The main goal of the motion capture system is to record and determine the 3D position and orientation of a wireless 3D controller using low-cost inertial and vision sensors. In designing such a system, it is very important to identify the main chal-

lenges and issues involved in accomplishing the primary goal. The main challenges in the design of the proposed system can be defined as follows:

Sensor Error – There are a number of different types of errors associated with inertial sensors such as rate gyros and accelerometers. As described in Chapter 2, inertial sensors do not measure position and orientation directly. Rate gyros measure angular velocity and accelerometers measure linear acceleration. To obtain actual position and orientation, it is necessary to perform numerical integration on the raw data acquired by the accelerometers and rate gyros respectively. Therefore, measurement error accumulates over time, resulting in a rapid degradation of tracking accuracy. Methods to reduce error accumulation is required for the system to perform with a reasonable level of accuracy.

Change in Coordinate Frames – Inertial sensors are capable of measuring only relative motion. As such, the measurements made by the inertial sensors are with respect to the 3D controller upon which the sensors are mounted. Therefore, a change in the orientation of the 3D controller causes a change in the orientation of the inertial sensors. This is problematic as the data measured by the inertial sensors will be with respect to the new coordinate frame. Therefore, methods to transform the measured data from the different coordinate frames to a common coordinate frame is required to determine the absolute position of the 3D controller.

Sensor Fusion – The motion of the same 3D controller is measured by different types of inertial sensors as well as the camera system. Therefore, a method to combine the data gathered from different sensor sources is needed to produce

information that is more reliable and more detailed than that produced by the individual sensor devices.

Visual Tracking – It is necessary to extract position information from the visual data acquired by the camera system. Therefore, the system must detect the 3D controller from the acquired visual data as well as determine its absolute position in an accurate and robust manner.

By defining the primary challenges, the proposed system can then be designed to address each of these challenges in an effective and efficient manner.

3.2 Structural Overview

The proposed system utilizes both hardware and software components to determine the final 3D position and orientation of the wireless 3D controller. The hardware used is responsible for acquiring sensory data about the wireless 3D controller, while the software is responsible for transforming the sensory data into usable 3D motion information.

3.2.1 Hardware

An overview of the hardware setup of the proposed system is shown in Figure 3.1. The proposed motion capture system consists of three main hardware components. The first component is the camera system, which acquires visual data about the 3D controller with respect to the surrounding environment. For the purpose of the proposed system, a single digital video camera was used to provide 2-D video feedback to the PC processing system. This is reasonable for consumer-level, human-

computer interfacing applications such as video game controllers and pen-based input devices since the motion of the input devices often follow along a 2-D plane at a close to medium range. For full 3D motion feedback, two or more digital video cameras must be placed in precise locations to perform accurate triangulation. However, such a complicated setup makes it difficult to integrate a multiple camera system into a typical consumer-level environment, such as an office or a home. Therefore, a single camera system is better suited for consumer-level 3D controller tracking applications. The camera is positioned such that its optical axis is parallel to the ground.

The second component of the motion capture system is the wireless 3D controller, which is held by the human user and used to interface with a given application. Applications that are well-suited for this type of system include applications that utilize pen-based input devices and video games that support wireless 3D controllers. These applications benefit from the greater degree of interaction that the proposed system provides. A general layout of the wireless 3D controller is illustrated in Figure 3.2. A passive spherical marker is mounted to the front of the wireless 3D controller. This marker allows the camera system to track the position of the 3D controller. A series of miniature inertial sensors are embedded into the wireless 3D controller to acquire 3D motion data with 6 degrees of freedom. The set of inertial sensors is referred to as the inertial measurement unit (IMU). This unit is described in further detail in Chapter 4.

The third and final component of the motion capture system is the PC processing system, which receives visual data from the camera system and inertial data from the IMU and processes it into a final set of 3D position and orientation coordinates. The details of the software in the PC processing system is presented in

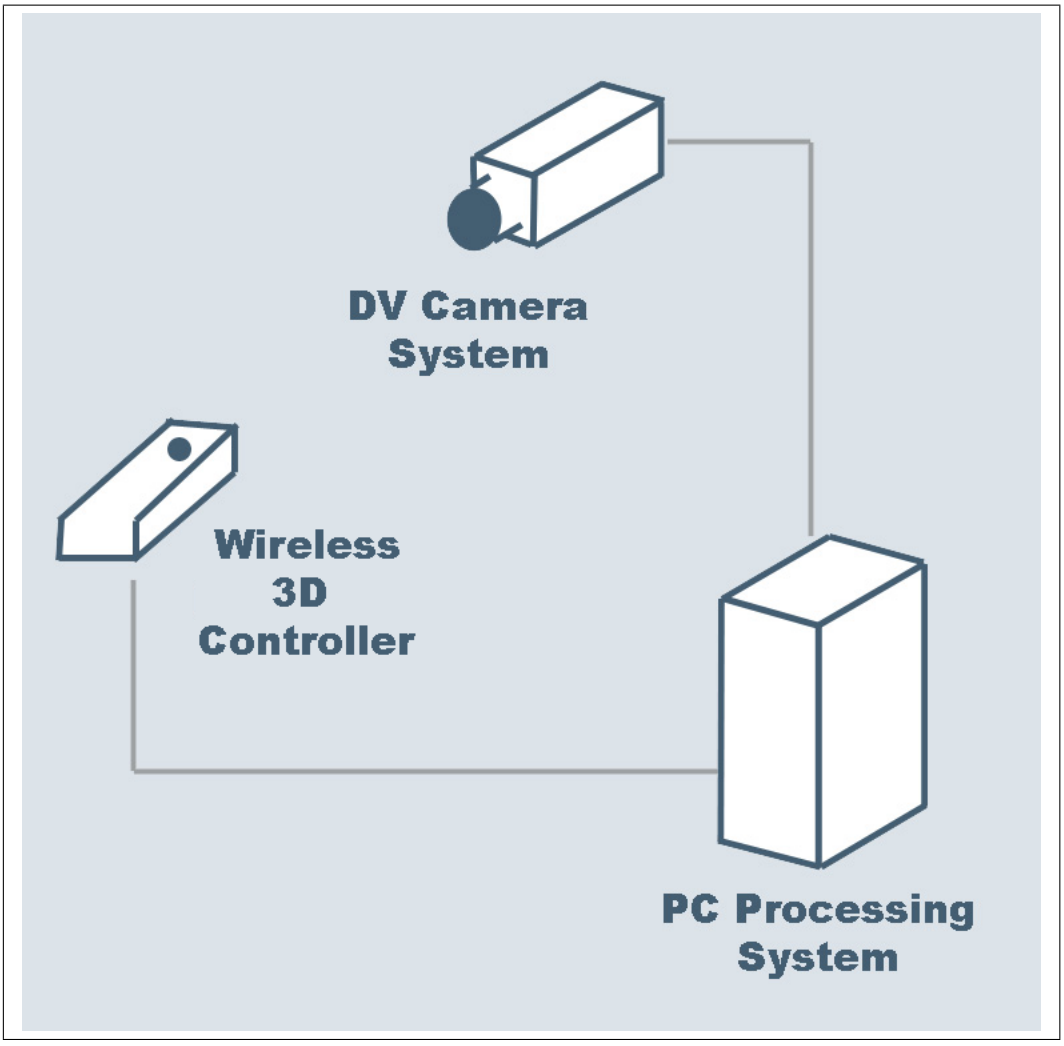

Figure 3.1: Hardware setup of the proposed motion capture system

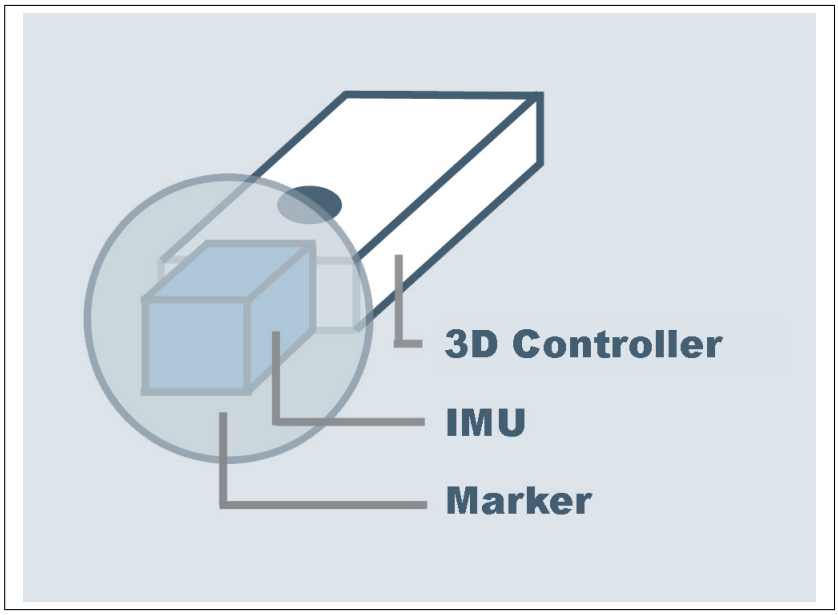

Figure 3.2: Setup of the wireless 3D controller

the following section.

3.2.2 Software

The software system executes on the PC processing system and it is responsible for taking the raw visual data acquired from the camera system and the raw inertial data from the IMU and processing it into the final set of 3D position and orientation coordinates. The software architecture of the proposed system is modularized. Each component in the software system is designed to address one or more issues described in Section 3.1. Such a design allows for the removal and addition of different sensors, in terms of quantity and modality. Furthermore, different filtering and processing techniques can be added to the system depending on factors such as cost, equipment accuracy, and processing power. An overview of the layout is

shown in Figure 3.3.

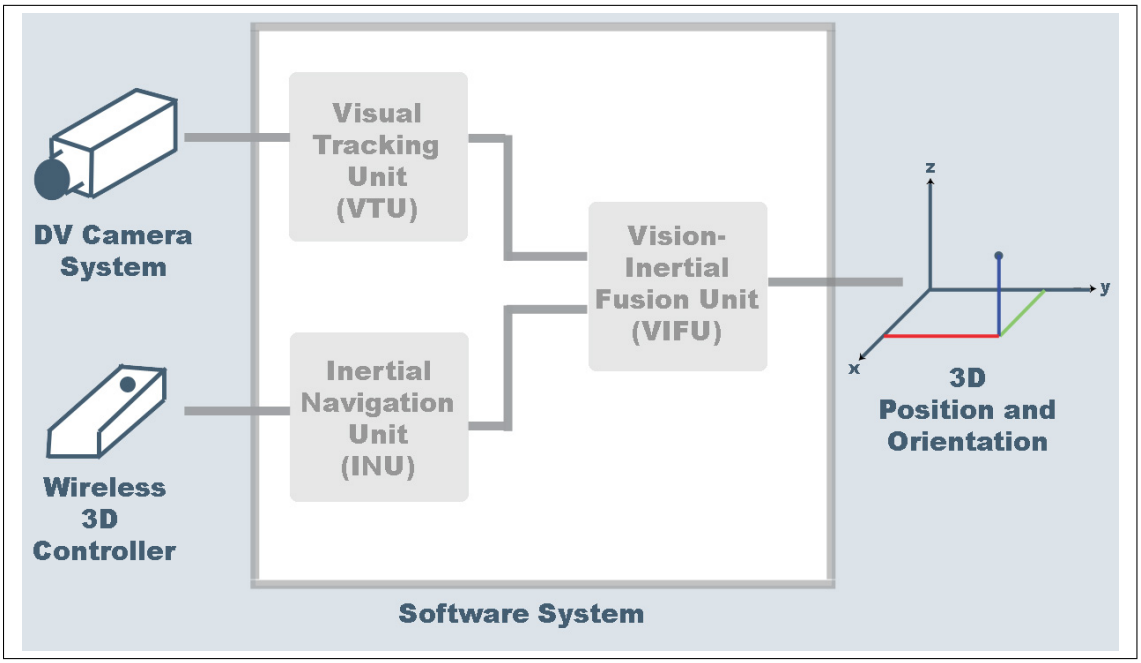

Figure 3.3: Overall software architecture of the proposed motion capture system

The software system in the proposed motion capture system consists of three main software components. The first component is the inertial navigation unit (INU), which is responsible for taking raw 3D inertial data from the IMU and transforming it into more consistent 3D position and orientation coordinates. To achieve this goal, the INU must be capable of performing three main tasks. First, it must take the raw inertial data and transform it into a consistent frame of reference. Second, it must attempt to filter noise from the raw inertial data to reduce error accumulation. Finally, it must take the linear acceleration and angular velocity information acquired by the IMU and convert it to position and orientation coordinates. The techniques used in the INU to perform these tasks are described in further detail in Chapter 5.

The second component of the software system is the visual tracking unit (VTU), which is responsible for taking the raw visual data from the camera system and extracting the 3D position of the wireless 3D controller. The VTU must be capable of detecting and distinguishing the marker on the 3D controller from the surrounding environment. Furthermore, based on the location of the detected marker in the visual data the VTU must also be able to estimate the absolute location of the marker in the real world. The techniques used in the VTU to perform these tasks are described in further detail in Chapter 6.

The third and final component of the software system is the vision-inertial fusion unit (VIFU). This unit is responsible for taking the processed 3D motion data from the IMU and the VTU and combining them into a final set of 3D position and orientation coordinates that is more detailed and stable than that obtained from either of the individual sources. This processing involves using the individual strengths of vision and inertial sensors to overcome the individual weaknesses of each technique. The techniques used in the VIFU to accomplish this are described in further detail in Chapter 7.

Chapter 4

Inertial Measurement Unit (IMU)

This chapter describes in detail the overall design and performance analysis of the inertial measurement unit (IMU). Introductions to inertial sensors, coordinate systems and frames of reference are presented. These topics are essential to a complete understanding of inertial sensor systems. A structural overview of the IMU is then presented. The sources of error associated with inertial sensors are presented, along with an error model which can then be used in the design of error reduction and correction techniques. The results are presented for the error evaluation performed on the gyro sensors and accelerometers in both static and dynamic situations. The analysis and performance evaluation aids in the determination of the limitations of the individual sensors in real-world situations.

4.1 Introduction

An inertial sensor is a device that measures motion based on the general principles of Newton's Laws of Motion. Newton's First Law of Motion states that an object in a state of uniform motion tends to remain in that state of motion unless acted upon by an unbalanced external force. By measuring the unbalanced force exerted on the object, the motion of the system can be deduced in a number of different ways. The two types of sensors that are most widely used in inertial motion sensing are accelerometers and gyro sensors.

Accelerometers are inertial sensor devices designed to measure linear acceleration. This is accomplished by measuring the force exerted on the sensor device and calculating the corresponding acceleration based on the measured force. Based on the calculated acceleration, the relative motion of the object can be determined. Linear velocity can be obtained by integrating the acceleration of the object. By performing a second integration, the position of the object can be determined. A number of different types of accelerometers are available. Of particular interest in recent years are accelerometers based on MEMS technology. Such devices are small, robust, and can be manufactured at a low cost. MEMS accelerometers such as those produced by Kionix [Kio06] are based on the principle of differential capacitance. A sensing element within the accelerometer moves in relationship with a fixed element. When the sensing element moves, its distance from the fixed element changes and this results in a change in electrical capacitance. This change in capacitance is then measured by the device and converted into a signal that is proportional to the acceleration of the device.

Gyro sensors are inertial sensor devices that measure angular velocity. Similar to accelerometers, gyro sensors measure the externally applied force and converts

the force into the corresponding angular velocity. This can then be used to determine the orientation of the sensor by integrating the measured angular velocity. A number of different types of gyro sensors have been developed, such as spinning gyro sensors, laser gyro sensors, and vibrating gyro sensors. Of particular interest are vibrating gyro sensors based on MEMS [ADBW02] and piezoelectric technology [Boy05]. Vibrating gyro sensors can be made small, stable, and reliable. Vibrating gyro sensors utilize the Coriolis effect. In steady state, the sensing element of the gyro sensor is forced to vibrate in a particular direction at a high frequency. When angular rotation occurs, a Coriolis force is exerted and causes the sensing element of the gyro sensor to move in a perpendicular direction to the vibration direction. This produces a current that is proportional to the angular velocity of the object. The operation of a piezoelectric-based gyro sensor is illustrated in Figure 4.1.

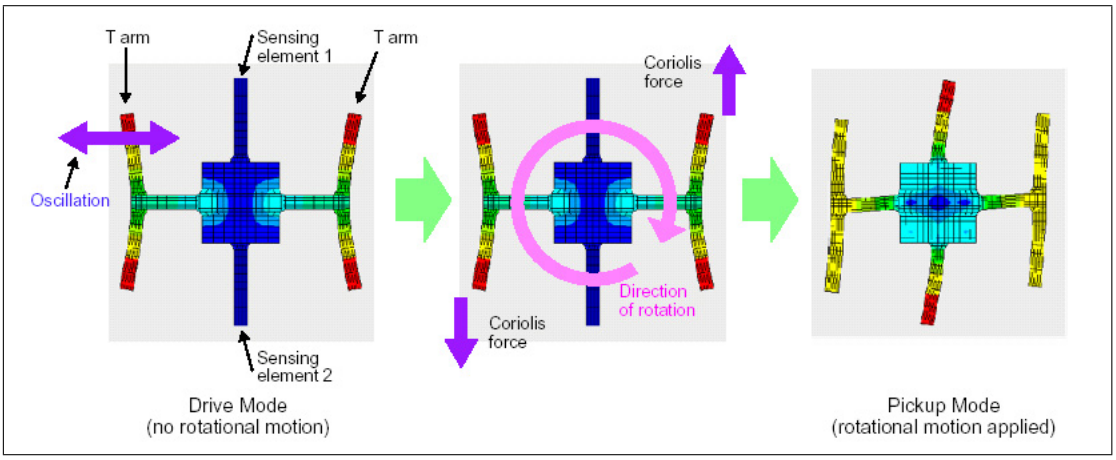

Figure 4.1: Operation of a piezoelectric-based vibrating gryo sensor (Courtesy of Epson)

It is important to note that, while both gyro sensors and accelerometers can be used to measure position and orientation respectively, neither measure position

and orientation in a direct manner. Therefore, it is necessary to further process the inertial data obtained from the inertial sensors to obtain position and orientation information.

4.2 Background Theory

Before describing the underlying setup of the IMU, it is important to provide a brief introduction to the fundamentals of coordinate systems to fully understand the measured data. In a common 3D coordinate system at an arbitrary frame of reference, the position of an object in 3D space is defined by a tri-axis system which consists of the x-axis, y-axis, and z-axis. A typical 3D coordinate system is illustrated in Figure 4.2.

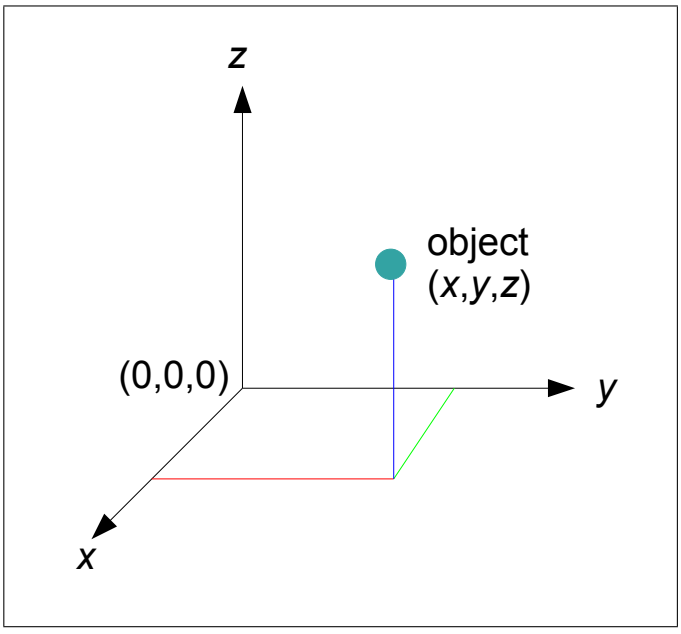

Figure 4.2: 3D tri-axis coordinate system

The orientation of an object in 3D space can be similarly defined using an orientation system based on the above tri-axis system. This orientation system consists of three parameters: i) roll, ii) pitch, and iii) yaw. Roll refers to a change in orientation about the x-axis. Pitch refers to an orientation change about the y-axis. Yaw refers to an orientation change about the z-axis. Positive values indicate counter clockwise rotations about the corresponding axis. The aforementioned orientation system is commonly represented using Euler angles by defining overall orientation as an ordered combination of rotations using three angles (α, β, γ). A rotation about the x-axis is denoted by α. A rotation about the y-axis is denoted by β. Finally, a rotation about the z-axis is denoted by γ. This orientation system representation is shown in Figure 4.3. Hence, a complete description of an object's motion can be summarized using six parameters (x,y,z for position, and α, β, γ for orientation).

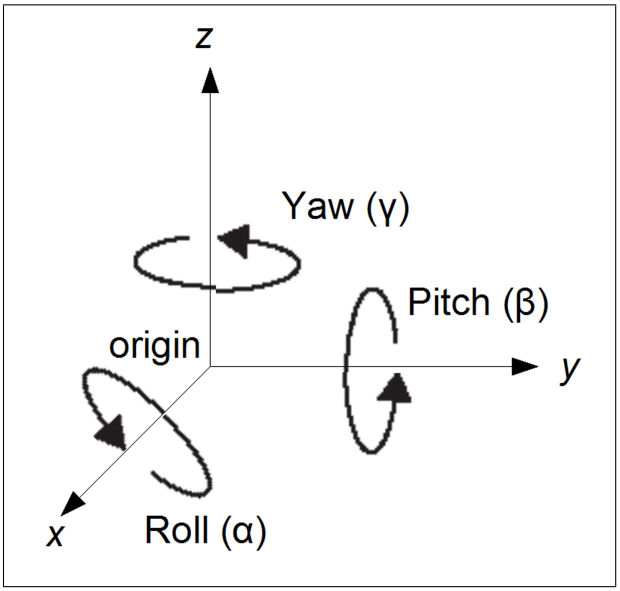

Figure 4.3: 3D orientation as represented using Euler angles

It is also necessary to provide an explanation on the different frames of reference used in the proposed motion capture system. This is because data acquired from the different sensor components of the proposed system are collected in different frames of reference. This makes it necessary to understand the different frames of reference used so that the acquired data can be brought into a single frame of reference for the purpose of data fusion. Two coordinate frames of reference are used in the proposed motion capture system: i) the device frame, and ii) the camera frame.

In the device frame of reference, the origin of the coordinate system is located at the center of gravity of the IMU. The x-axis is pointed out of the front of the wireless 3D controller. The y-axis points out of the left of the 3D controller and the z-axis points out of the top of the controller. The device frame of reference is illustrated in Figure 4.4.

In the camera frame of reference, the origin of the coordinate system is located at the projection center of the camera system. The x-axis is points towards the camera from the image plane. The y-axis points right from the camera's perspective and and the z-axis points upwards from the camera's perspective. The camera frame of reference is illustrated in Figure 4.5. The coordinate transformation from the device frame of reference to the camera frame of reference is discussed in Section 5.3.1 and Section 5.4.2 for the gyro sensors and accelerometers, respectively.

4.3 IMU Structural Overview

The IMU consists of six inertial sensors: three gyro sensors and three accelerometers. The three gyro sensors are mounted in a tri-axis configuration to measure

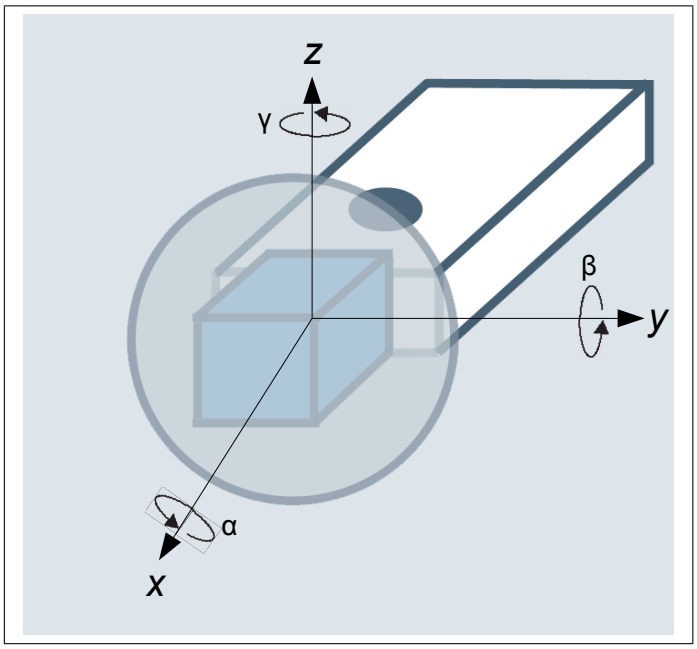

Figure 4.4: Device frame of reference

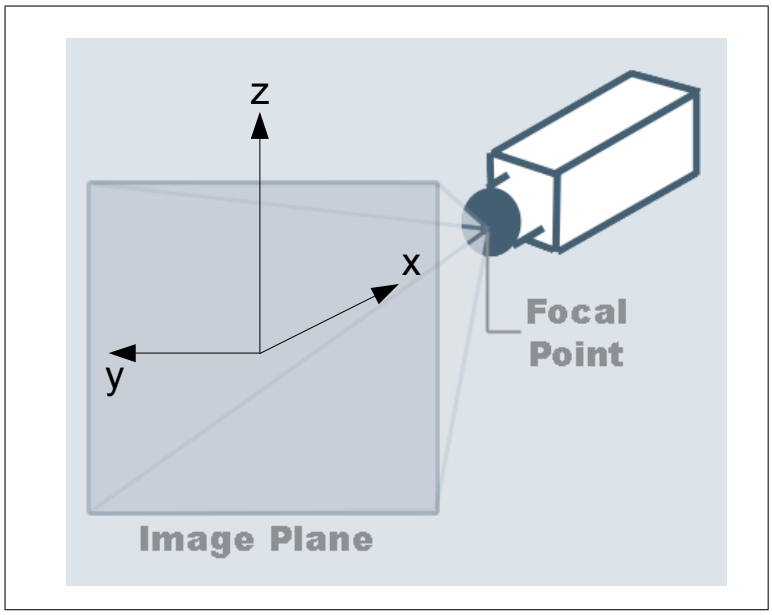

Figure 4.5: Camera frame of reference

angular velocity at three degrees of freedom in the device frame: i) roll, ii) pitch, and iii) yaw. The three accelerometers are also mounted in a tri-axis configuration to measure linear acceleration at three degrees of freedom in the device frame: i) x-axis, ii) y-axis, and iii) z-axis. By combining the three gyro sensors and the three accelerometers, the IMU can measure motion with six degrees of freedom. The IMU is embedded in the center of the marker at the front of the wireless 3D controller.

For the test implementation of the motion capture system, a MicroStrain G-Link 2.4 GHz Wireless Accelerometer [Mic07] was provided courtesy of Epson Corporation to measure linear acceleration in 3D space. The accelerometers used within the device are based on MEMS technology and have an acceleration range of $\pm$2G and a maximum sampling rate of 2,048 sweeps per second. Epson Corporation also provided an InterSense Wireless InertiaCube3 [Int07] for the purpose of measuring angular motion in 3D space. Based on the specifications provided by InterSense, the device contains three gyro sensors and is capable of obtaining angular orientation with a RMS accuracy of 0.25° for pitch at a temperature of 25 °C without system enhancements enabled. All internal optimization settings for the device are turned off to provide the best possible representation of the raw data from the built-in sensors.

4.4 Sources of Error and Error Model

One of the main caveats to using inertial sensors for motion capture purpose is the instability of such systems in long-term situations as a result of error accumulation. Inertial sensors such as accelerometers and gyro sensors do not measure position or orientation directly. To obtain the position and orientation of an object in

3D space, integration must be performed on the measured data from the inertial sensors. This is particularly problematic for accelerometers since the acquired data must be integrated twice to obtain position information. Errors in acceleration measurement increase the position error quadratically. Therefore, it is necessary to reduce and correct the associated error to obtain accurate position information.

To develop proper error filtering and correction methods, it is necessary to identify and understand the underlying sources of error associated with the inertial sensors used in the IMU. This allows for the formulation of error models for representing these sources of error. Sources of error associated with inertial sensors such as accelerometers and gyro sensors can be generalized into four categories: i) scaling factor error, ii) gravity-related error, iii) manufacturing-related error, and iv) time-varying error. Both gyro sensors and accelerometers are susceptible to scaling factor errors, manufacturing-related errors, and time-varying errors, while gravity-related errors apply to accelerometers only.

It is typically the case that the raw data acquired from an inertial sensor is proportional to but not equal to the actual motion. It is necessary to scale the measured data by a scaling factor to obtain the actual motion. A suggested scaling factor is usually not provided by the manufacturer. Therefore, a scaling factor must be determined experimentally for a specific sensor. An incorrect scaling factor or a change in scaling factor results in an error that is proportional to the difference between the actual and incorrect scaling factors. The sensor model of an inertial sensor with a scaling factor error can be represented as:

$$x_{\text{measured}} = (1 + e_{\text{scale}})x_{\text{actual}} \tag{4.1}$$

where x_{measured} is the measured sensor output, e_{scale} is the scaling factor error, and

x_{actual} is the actual sensor output. Fortunately, it was found in [GE04] that external factors have minimal effects on the scaling factor of inertial sensors. For a simplified error model, it is not required to account for scaling factor errors.

The second source of error is related to changes in local gravitational effects. As previously discussed, accelerometers measure external forces directly but do not measure acceleration directly. The force of acceleration can be determined as follows:

$$a_{\text{actual}} = a_{\text{measured}} - g \tag{4.2}$$

where a_{actual} is the actual acceleration force, a_{measured} is the measured acceleration force, and g is the gravitational force acting on the sensor. It is necessary to remove the effects of gravity to obtain the actual acceleration of the object. Gravitational force is often represented by the gravitational constant. However, gravitational force actually varies depending on the location of the object. As a result, the use of a fixed gravitational term results in inaccurate acceleration measurements. Fortunately, this form of error can be corrected during the calibration of the proposed motion capture system by measuring the actual gravitational force at the specific location and using it to remove gravitational effects. Therefore, gravitational effects can be taken into account during the calibration process.

The third source of error is related to particularities in the manufacturing process of the individual sensors. Defects and imperfections in the inertial sensor devices can lead to measurement biases that result in error accumulation. A related source of error is the degradation of device performance due to wear. Over time, inertial sensors within a device may become misaligned or damaged from excessive use. This type of error must be taken into account in the error model and can be modeled effectively as a constant offset e_{constant}.

The final source of error is related to error sources that vary over time. These include electrical noise, sampling noise, and device sensitivity errors. To simplify the overall error model, time-varying error sources are grouped into two categories: i) sampling noise ($e_{\text{sampling}}(t)$), and ii) non-sampling noise ($e_{\text{vary}}(t)$). This is sufficient for the proposed motion capture system because a vision-based system with good long-term stability is used to improve and complement the results acquired from the IMU.

Based on the above descriptions, a general error model that is suitable for both the gyro sensors and accelerometers used in the proposed motion capture system can be expressed as:

$$x_{\text{measured}} = x_{\text{actual}} + e \tag{4.3}$$

$$e = e_{\text{constant}} + e_{\text{vary}}(t) + e_{\text{sampling}}(t) \tag{4.4}$$

where x_{measured} is the measured value, x_{actual} is the actual value, e is the overall error, e_{constant} is the constant bias, $e_{\text{vary}}(t)$ is the time-varying error bias, and $e_{\text{sampling}}(t)$ is the sampling error.

4.5 Rate Gyro Error Evaluation

A total of four tests were performed to validate the accuracy of the gyro sensor when compared with the specifications provided by the manufacturer. The tests were designed to test a variety of different scenarios, with two controlled tests that can be easily replicated and two uncontrolled tests based on random motion. The uncontrolled tests are more representative of real-world scenarios and therefore reflect the actual real-world performance of the device to a greater degree. Ten

trials were performed for each of the tests to improve the statistical accuracy of the results. Below is a description of each of the four tests:

Test 1: In this controlled test, the pitch orientation of the device is changed by a total of 10° in 3 s, while the yaw and roll orientations are left unchanged. This test is performed to test the device under motion in a single plane and to validate whether the device is capable of producing accurate results under small orientation changes.

Test 2: In this controlled test, the pitch orientation of the device is changed by a total of 360°, while the yaw and roll orientations are left unchanged. This results in a net orientation change of 0° in pitch. This test is performed to test the device to validate whether the device is capable of producing accurate results under large changes in orientation.

Test 3: In this uncontrolled test, the pitch, yaw, and roll orientations of the device are changed continuously in a random fashion at a random rate for a period of 10 s. By controlling the final pitch orientation of the testing apparatus, the net orientation change is 30° in terms of pitch orientation. This test is performed to test the device to validate whether the device is capable of maintaining accurate orientation states under sporadic rotational changes over a very short period of time. This test validates the short-term reliability of the gyro sensor device.

Test 4: In this uncontrolled test, the pitch, yaw, and roll orientations of the device are changed continuously in a random fashion at a random rate for a period of 2 minutes. By controlling the final pitch orientation of the testing apparatus, the net orientation change is 30° in terms of pitch orientation. This test is performed to test the device to validate whether the device is capable of maintaining accurate orientation states under sporadic rotational changes over a longer period of time

when compared to the previous test. Furthermore, the 10 trials for this test are performed consecutively without resetting the device to evaluate the accumulated error over a long period of time. The total testing time was measured to be 26 minutes from the start of the first trial to the end of the last trial. This test validates the long-term reliability of the sensor device.

4.5.1 Experimental Results

A summary of the orientation accuracy results of Tests 1 to 4 is shown in Table 4.1. It can be observed that the gyro sensor device performs well within the specifications in three of the four test scenarios. In the first test, the RMS error is very small and within range of the provided specifications. In the second and third tests, the RMS error is higher than the first test. However, it is still very small and within the range of the provided specifications. From the perspective of a consumer-level application, the differences in RMS error amongst the first three tests can be considered negligible. Therefore, it is evident that the sensor device is capable of producing accurate results in short-term scenarios in the presence of different orientation changes and different sporadic motions.

Test No.	**Actual Net Orientation (Degrees)**	**Mean Measured Orientation (Degrees)**	**RMS Error (Degrees)**	**Error Standard Deviation (Degrees)**	**Accumulated Error (Degrees)**
1	10	9.910	0.3034	0.1704	-
2	0	0.341	0.4341	0.2831	-
3	30	30.139	0.3587	0.2229	-
4	30	29.805	0.8393	0.4329	6.410

Table 4.1: Summary of orientation accuracy tests

Based on the accuracy results of Test 4, it can be observed that the resulting RMS error is noticeably higher than that provided by InterSense. It can also be observed that the accumulated error is noticeable over the test period of 26 minutes. Furthermore, the accumulated error result validates that the error of the gyro sensors increases linearly with respect to time. While the accumulated error of the device can be considered small for a consumer-level application such as the proposed motion capture system, this does indicate that the accumulated error begins to have a noticeable influence on orientation accuracy when the usage period is extended to a longer period of time (i.e., hours). As such, it is necessary to provide the user with a means to recalibrate the wireless 3D controller after an extended period of usage to maintain accuracy. The error accumulation of the gyro sensor device is linear and given the accuracy of the device and the accuracy needed for the application it can be used for over an hour without the need for recalibration in its current state. Simple noise filtering techniques can be used to further extend this time period without recalibration.

It is evident from the experimental results that low-cost gyro sensor devices such as the InterSense Wireless InertiaCube3 are capable of producing accurate orientation measurements. The device is relatively stable over a reasonably long period of time without aid or recalibration. This makes it well-suited for use in the proposed motion capture system, since the vision system is not capable of providing useful information regarding the orientation of the 3D controller.

4.6 Accelerometer Error Evaluation

A total of four tests were performed to validate the accuracy of the accelerometer device under a number of different scenarios. The four tests are designed to evaluate the static positioning accuracy of the device over an extended period of time. The relative position of the device based on the measured acceleration was calculated by finding the double integral of the measured data. The constant bias was estimated from long-term data and subtracted from the acceleration data. A number of trials were performed for each test to improve statistical accuracy of the results. Each test was conducted for a maximum of 65,500 sweeps due to the memory storage limitations of the device. A description of the tests are provided as follows:

Test 1: In this static position accuracy test, the device is left in a fixed location with no external forces being exerted on the device. The device is configured to measure a total of 65,500 sweeps at 2,048 sweeps/second, resulting in a total measurement time period of 31.98 s. This test is performed to evaluate the accumulated error of the device and its effect on position measurement over a shorter period of time at a high sampling rate. A total of 10 trials were conducted.

Test 2: In this static position accuracy test, the device is left in a fixed location with no external forces being exerted on the device. The device is configured to measure for 65,500 sweeps at 1,024 sweeps/second, resulting in a total measurement time period of 63.96 s. A total of 10 trials were conducted.

Test 3: In this static position accuracy test, the device is left in a fixed location with no external forces being exerted on the device. The device is configured to measure for 65,500 sweeps at 512 sweeps/second, resulting in a total measurement time period of 127.93 s. A total of 10 trials were conducted.

Test 4: In this static position accuracy test, the device is left in a fixed location with no external forces being exerted on the device. The device is configured to measure for 65,500 sweeps at 256 sweeps/second, resulting in a total measurement time period of 255.86 s. This test is performed to evaluate the accumulated error of the device and its effect on position measurement over a longer period of time at a low sampling rate. A total of 10 trials were conducted.

4.6.1 Experimental Results

A summary of the position accuracy results of Tests 1 to 4 is shown in Table 4.2. It can be observed that the accelerometer device performs poorly in all tests when used to determine the position of an object without any additional aid or filtering. In the first test, the accumulated error is very large over a very short period of time when compared to that of the gyro sensor device. This is further reinforced by the second test, where the accumulated error exceeds a meter in a little over a minute.

Test No.	Mean Accumulated Error (m)	Error Standard Deviation (m)
1	0.1560	0.0112
2	1.5400	0.1784
3	2.6885	0.4014
4	8.0794	0.7622

Table 4.2: Summary of position accuracy tests

A sample test trial from Test 2 is illustrated in Figure 4.6. It can be seen that the error accumulation in terms of position grows in a quadratic manner. Therefore, it is evident that the accelerometer device is unable to produce accurate data over an extended period of time for the purpose of 3D motion tracking if unaided by a

secondary device. Fortunately, the vision system in the proposed motion capture system can be used to provide error correction for the inertial system.

It is evident that the accelerometer device is capable of acquiring many samples over a short period of time, resulting in a detailed description of the motion of an object. However, it is also clear that it is highly unstable in the long-term when used for determining position information. This indicates that error filtering and correction is necessary if one desires highly detailed and accurate results. These techniques are discussed in Chapter 5 and Chapter 7.

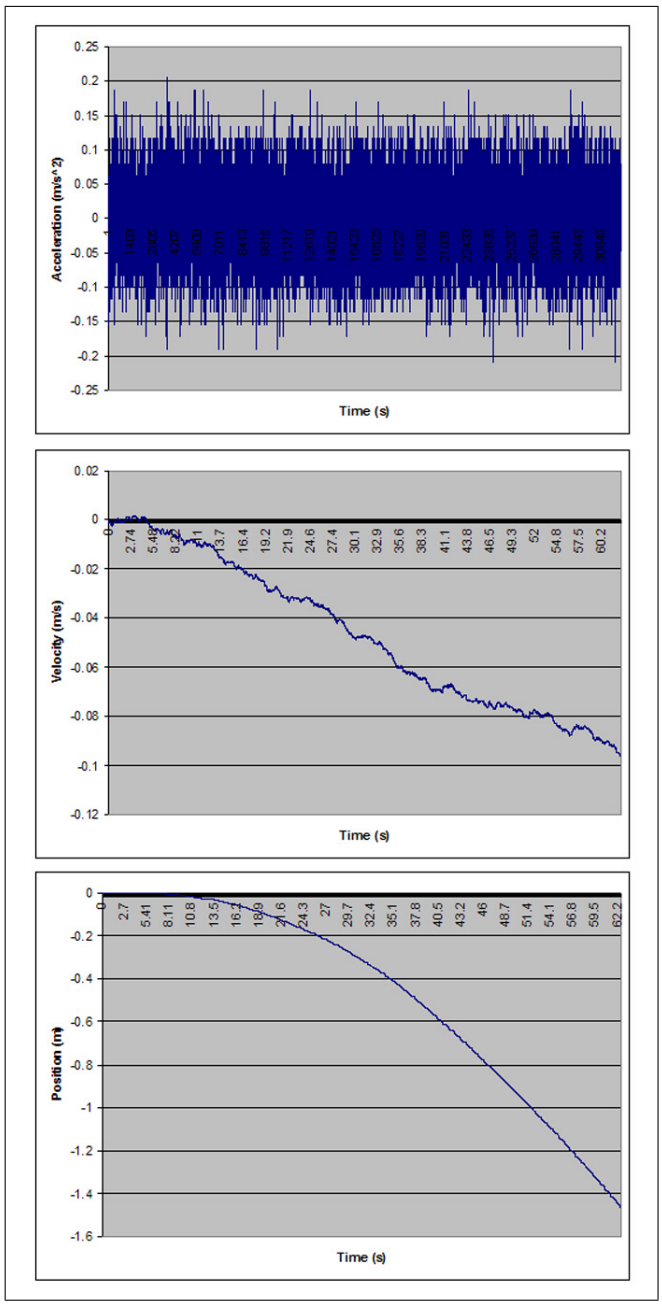

Figure 4.6: Sample test trial from position accuracy tests

Chapter 5

Inertial Navigation Unit (INU)

This chapter describes in detail the overall design of the inertial navigation unit (INU). The first section presents an introduction to inertial navigation systems. The next section provides a structural overview of the INU. The data transformation systems used for gyro and accelerometer data are described in Section 5.3 and Section 5.4, respectively. Section 5.3.1 provides a discussion on calibrating the angular velocity data from the device frame of reference with the camera frame of reference. Section 5.3.2 describes integration and error reduction techniques used to convert angular velocity information into orientation information. Section 5.4.1 describes the error reduction performed for the accelerometer data in the INU. Section 5.4.2 describes the theory used to transform linear acceleration data from the device frame of reference to the camera frame of reference. Section 5.4.3 presents the integration techniques used to convert linear acceleration information into position information.

5.1 Introduction

An inertial navigation system (INS) is a system that computes motion information using measurements made by inertial sensor devices such as accelerometers and gyro sensors. To accomplish this goal, the INS must be capable of performing a number of important tasks. Navigation systems such as GPS and optical systems [KGK02] calculate position and orientation information in a direct manner for the purpose of deriving other motion characteristics such as velocity and acceleration. Unlike these systems, an INS must deduce position and orientation information in an indirect manner from the linear acceleration and angular velocity information provided by the inertial sensor devices. This is accomplished in an INS by performing a double integration on the linear acceleration data to obtain position and a single integration on the angular velocity data to obtain orientation.

Inertial sensors are capable of measuring only relative motion. Data obtained from these inertial devices can be said to be in a device frame of reference. For the proposed system, it is necessary to obtain absolute position and orientation information from a camera frame of reference. Therefore, the INS is responsible for transforming the inertial data from the device frame of reference to the camera frame of reference. Finally, due to the errors associated with inertial sensor devices (particularly accelerometers), the INS must also provide error reduction capabilities for the resulting position and orientation information to be useful.

5.2 INU Structural Overview

The INU used in the proposed motion capture system is implemented as part of the PC processing system. The general architecture of the INU is illustrated in Figure 5.1. The architecture of the INS is divided into two main components. The first component is the angular velocity processing unit, which is responsible for transforming the angular velocity data from the IMU into orientation information. This component is further divided into two subcomponents. The first subcomponent is responsible for calibrating the raw data from the device frame of reference with the camera frame of reference. The second subcomponent is responsible for performing integration and error reduction on the newly transformed data from the first subcomponent.

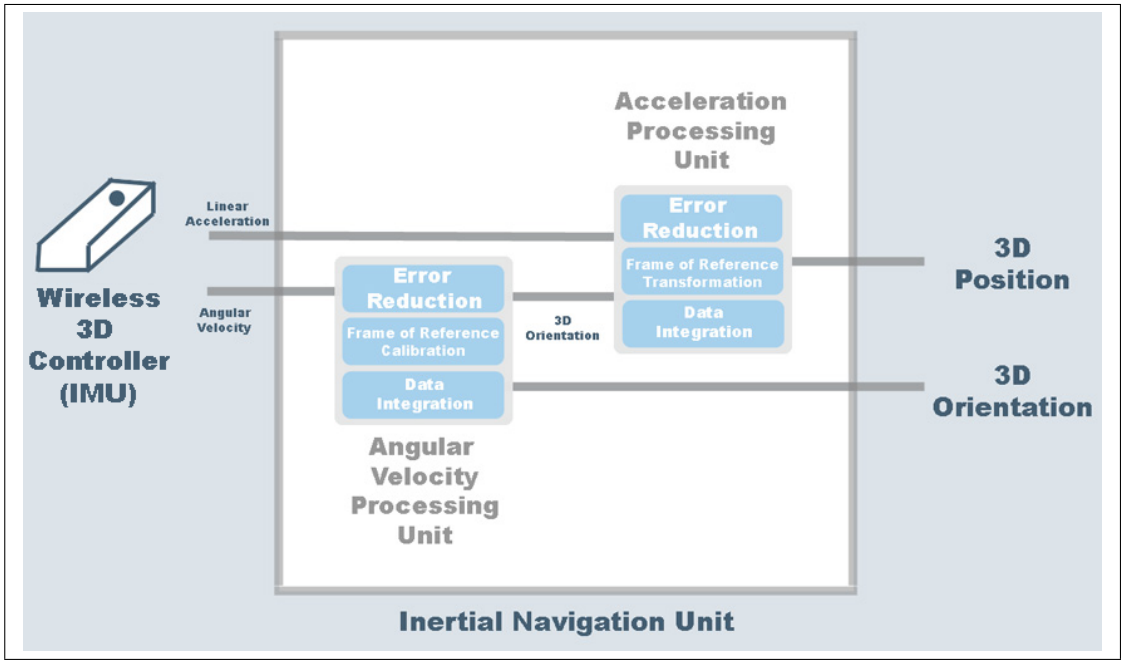

Figure 5.1: INU setup

The second component is the acceleration processing unit, which is responsible for transforming linear accelerometer data from the IMU into position information. The linear accelerometer processing unit is divided into two subcomponents. The first subcomponent utilizes the orientation information from the angular velocity processing unit to transform the linear acceleration data from the device frame of reference to the camera frame of reference. The second subcomponent then takes the transformed acceleration data and integrates the data to obtain position information. Furthermore, the second subcomponent is responsible for performing error reduction on the acceleration data.

5.3 Angular Velocity Processing Unit

The angular velocity processing unit takes angular velocity information from the gyro sensor device and transforms it into 3D orientation information.

5.3.1 Frame of Reference Calibration

To transform the angular velocity information from the device frame of reference to the camera frame of reference, it is necessary to know the initial orientation of the wireless 3D controller. This is accomplished through a device calibration process where the user is informed to hold the wireless 3D controller in a horizontal manner such that the bottom face of the device is parallel to the ground and the front of the device points towards the camera. This effectively aligns the device with the camera whose optical axis is set such that it runs parallel to the ground. A sample calibration alignment is illustrated in Figure 5.2. This orientation is then recorded as the origin orientation in the camera frame of reference.

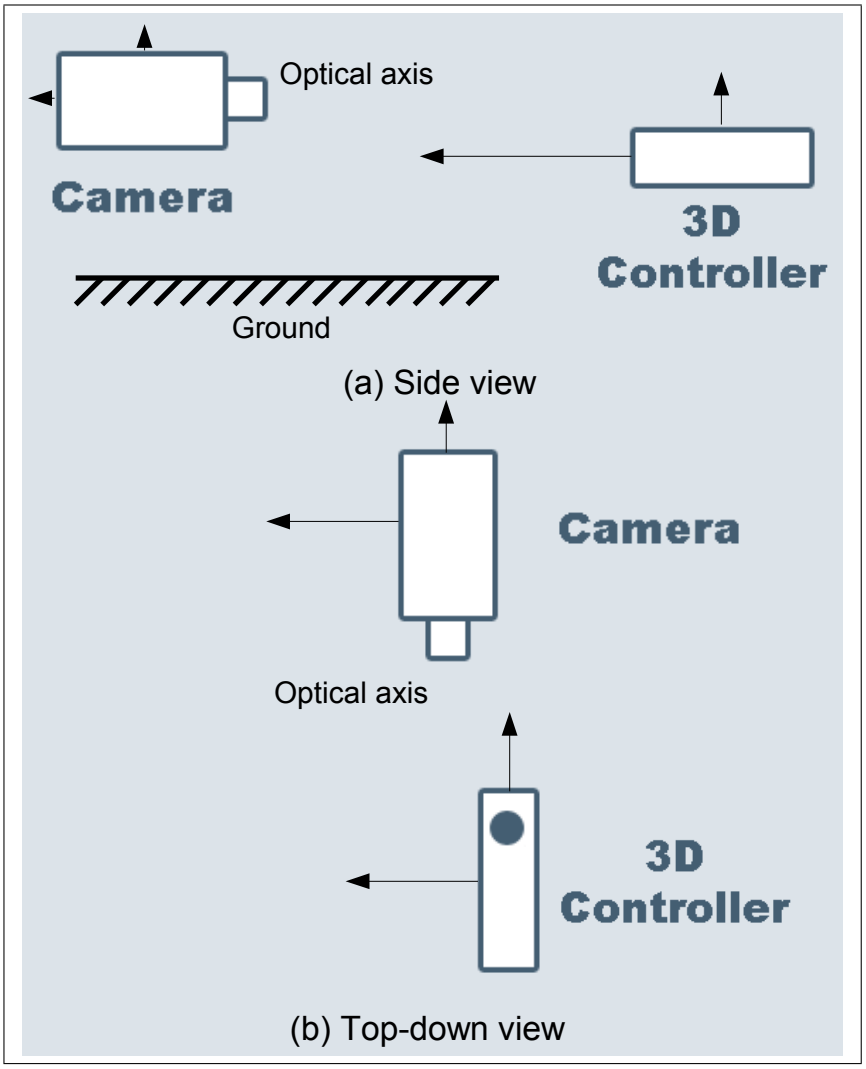

Figure 5.2: Sample calibration alignment

5.3.2 Data Integration and Error Reduction

Once the orientation of the device has been calibrated with the camera frame of reference, it is necessary to compute the orientation of the wireless 3D controller using the measured angular velocity from the IMU. This is accomplished by performing a single integration on the angular velocity data collected for roll, pitch, and yaw:

$$\alpha(t) = \int \omega_\alpha(t)dt \tag{5.1}$$

$$\beta(t) = \int \omega_\beta(t)dt \tag{5.2}$$

$$\gamma(t) = \int \omega_\gamma(t)dt \tag{5.3}$$

where $\omega_\alpha(t), \omega_\beta(t)$, and $\omega_\gamma(t)$ are the angular velocities for roll, pitch, and yaw, respectively at time t, and $\alpha(t), \beta(t)$, and $\gamma(t)$ are the roll, pitch, and yaw, respectively at time t.

Prior to performing integration on the measured angular velocity, it is necessary to remove the constant bias that corrupts the measured data. This is important because a constant bias in the angular velocity results in a linear error accumulation in the computed orientation over time. To remedy this, the wireless 3D controller is measured over a period of time during the calibration process to estimate the initial condition of the device without any external forces being applied. The constant bias can then be estimated as the average of the data obtained when the device is unaffected by external forces.

There are a number of different approaches suitable for performing the numerical integration operation. The most widely used approach to numerical integration

involves the use of Newton-Cotes formulas (e.g., Trapezoid rule, Simpson's rule, etc.). A more advanced approach to numerical integration involves the use of Gaussian quadratures (e.g., Gauss-Hermite, Gauss-Legendre, etc.), which provide greater flexibility (i.e., support for non-uniformly spaced samples) and accuracy at the cost of higher computational overhead than the Newton-Cotes formulas. Since data is acquired at equally spaced intervals by the IMU, the Newton-Cotes approach provides good accuracy at a low computational cost. For the proposed system, the Simpson's Rule was used to perform numerical integration on the inertial data as it provides a good balance between efficiency and accuracy, especially given that fact that the acquired data is read sequentially without further subsampling. Simpson's Rule approximates the area under a curve using a series of quadratic polynomials. The resulting formula for computing orientation from angular velocity for a specific axis (roll, pitch, yaw) is given by the following:

$$\int_0^n \theta(t)dt \approx \sum_{k=1}^{\frac{n-1}{2}} \frac{h}{3}\left[\omega(2k-1) + 4\omega(2k) + \omega(2k+1)\right] + O(h^5 f^{(4)}(k)) \tag{5.4}$$

where $h = \Delta t$ is the sampling period, θ is the orientation angle for a particular axis, and ω is the angular velocity for the chosen axis. The $O(h^5 f^{(4)}(k))$ term is a remainder term that is approximately 0 for small values of h.

5.4 Acceleration Processing Unit

The acceleration processing unit takes linear acceleration information from the accelerometer device and transforms it into 3D position information.

5.4.1 Error Reduction

Prior to performing a frame of reference transformation on the measured linear acceleration data, it is necessary to remove the constant bias that corrupts the measured data. This is important because a constant bias in the acceleration data results in an exponential error accumulation in the computed position over time. To remedy this, the wireless 3D controller is measured over a period of time during the calibration process to determine the initial condition of the device without any external forces being applied. To accomplish this, the effects of gravity are first subtracted from the measurements of the IMU. The constant bias can then be estimated as an average of the data obtained when the device is unaffected by external forces and subtracted from the acceleration data. The effect of constant bias removal is illustrated in Figure 5.3. It is clear from the figure that the accumulated error is significantly reduced after the constant bias removal process. Note that the vertical axis scale of the first figure is much greater than the vertical axis scale of the 2nd figure due to the accumulated error introduced by the constant bias.

5.4.2 Frame of Reference Transformation

The raw acceleration data from the IMU is acquired in the device frame of reference. As such, the data from IMU is able to describe relative motion and not absolute motion in the environment as needed by the motion capture system. Therefore, it is necessary to transform the linear acceleration information from the device frame of reference to the camera frame of reference. The first step is to determine the initial position of the device in the camera frame of reference to serve as the 3D position offset of the device. This is accomplished at the calibration stage, when

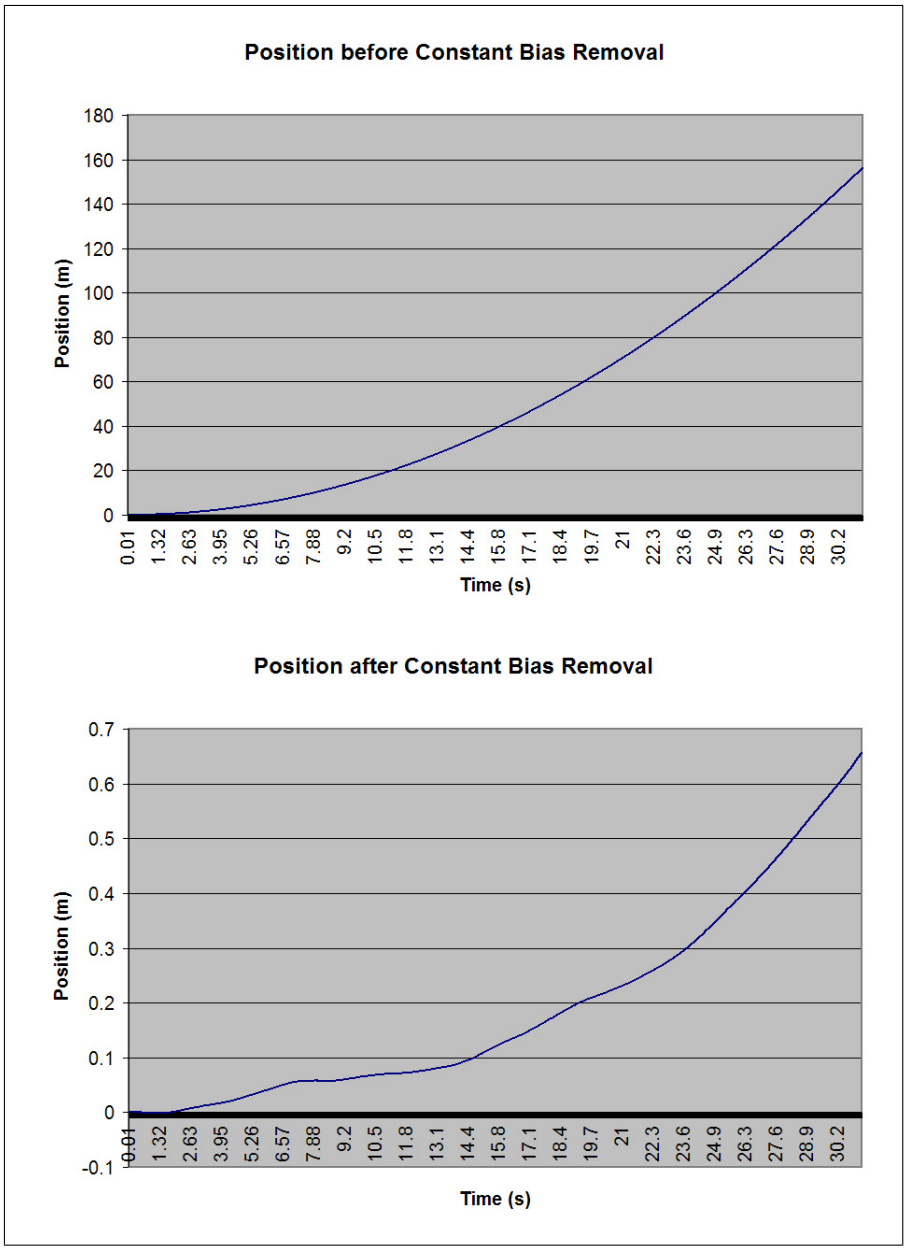

Figure 5.3: Effect of constant bias removal

the camera system determines the initial position of the device in the camera frame of reference. The initial position coordinates are denoted by (x_0,y_0,z_0).

The second step in transforming 3D acceleration data from the device frame of reference to the camera frame of reference is to determine the transformation model that relates the two frames of reference. This is accomplished through the use of 3D orientation data that was computed by the angular velocity processing unit. The transformation model from the camera frame of reference to the device frame of reference and vice versa at a particular point in time can be defined as an series of rotations performed in a consecutive fashion. In the case of Euler angles, the transformation model from the camera frame of reference to the device frame of reference can be represented as a sequence of yaw (γ), pitch (β), and roll (α). This is illustrated in Figure 5.4.

The net frame of reference transform from the camera frame of reference to the device frame of reference can be formulated as a direction cosine matrix (DCM) $R^{\text{device}}_{\text{camera}}$ as follows:

$$R^{\text{device}}_{\text{camera}} = R(\alpha)R(\beta)R(\gamma) \tag{5.5}$$

where

$$R(\alpha) = \begin{bmatrix} 1 & 0 & 0 \\ 0 & \cos(\alpha) & -\sin(\alpha) \\ 0 & \sin(\alpha) & \cos(\alpha) \end{bmatrix} \tag{5.6}$$

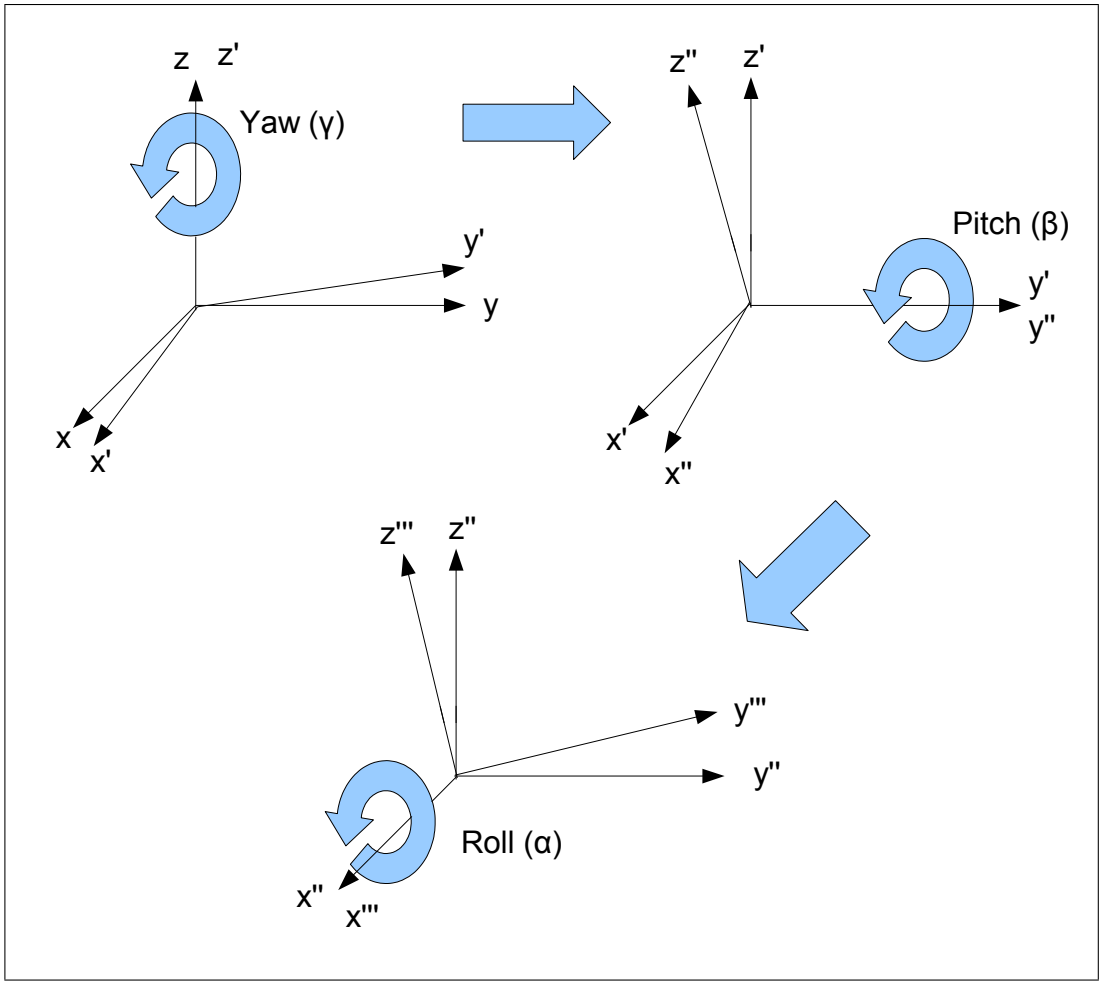

Figure 5.4: Frame of reference transform

$$R(\beta) = \begin{bmatrix} \cos(\beta) & 0 & \sin(\beta) \\ 0 & 1 & 0 \\ -\sin(\beta) & 0 & \cos(\beta) \end{bmatrix} \tag{5.7}$$

$$R(\gamma) = \begin{bmatrix} \cos(\gamma) & -\sin(\gamma) & 0 \\ \sin(\gamma) & \cos(\gamma) & 0 \\ 0 & 0 & 1 \end{bmatrix} \tag{5.8}$$

and positive angles indicate counter-clockwise rotations. Due to the orthogonal property of DCMs, the DCM that transforms data from the device frame of reference to the camera frame of reference can be computed as follows:

$$\begin{aligned} R_{\text{device}}^{\text{camera}} &= R(\gamma)^T R(\beta)^T R(\alpha)^T \\ &= \begin{bmatrix} \cos(\beta)\cos(\gamma) & \sin(\alpha)\sin(\beta)\cos(\gamma) + \cos(\alpha)\sin(\gamma) & \sin(\alpha)\sin(\gamma) - \cos(\alpha)\sin(\beta)\cos(\gamma) \\ -\cos(\beta)\sin(\gamma) & \cos(\alpha)\cos(\gamma) - \sin(\alpha)\sin(\beta)\sin(\gamma) & \cos(\alpha)\sin(\beta)\sin(\gamma) + \sin(\alpha)\cos(\gamma) \\ \sin(\beta) & -\sin(\alpha)\cos(\beta) & \cos(\alpha)\cos(\beta) \end{bmatrix} \end{aligned} \tag{5.9}$$

where the Euler angles are a function of time in the case of the proposed motion capture system. Therefore, the acceleration data from the three dimensions (a_x^{device},a_y^{device},a_z^{device}) can be transformed from the device frame to the camera frame at a particular time t using the DCM $R_{\text{device}}^{\text{camera}}$. Furthermore, the gravitational force g is subtracted from the acceleration in the z-axis to remove its effect on the system. The final overall transform can be represented as:

$$\begin{bmatrix} a_x^{\text{camera}}(t) \\ a_y^{\text{camera}}(t) \\ a_z^{\text{camera}}(t) \end{bmatrix} = R_{\text{device}}^{\text{camera}}(t) \begin{bmatrix} a_x^{\text{device}}(t) \\ a_y^{\text{device}}(t) \\ a_z^{\text{device}}(t) \end{bmatrix} - \begin{bmatrix} 0 \\ 0 \\ g \end{bmatrix} \tag{5.10}$$

5.4.3 Data Integration

Once the acceleration data has been transformed from the device frame of reference to the camera frame of reference, it is necessary to compute the position of the wireless 3D controller using the measured linear acceleration data from the IMU. This is accomplished by performing a double integration on the linear acceleration data collected for the x, y, and z-axes:

$$x(t) = \int\int a_x(t)dt^2 \tag{5.11}$$

$$y(t) = \int\int a_y(t)dt^2 \tag{5.12}$$

$$z(t) = \int\int a_z(t)dt^2 \tag{5.13}$$

where $a_x(t), s_y(t)$, and $a_z(t)$ are the linear acceleration in the camera frame of reference for the x, y, and z-axis respectively at time t, and $x(t), y(t)$, and $z(t)$ are the position coordinates at time t. As with the angular velocity processing unit, the Simpson's Rule approach to numerical integration is used to compute the position information. The resulting formula for computing position from acceleration for a specific axis (x, y, and z) is given by the following:

$$\int_0^n v(t)dt \approx \sum_{k=1}^{\frac{n-1}{2}} \frac{h}{3}\left[a(2k-1) + 4a(2k) + a(2k+1)\right] + O(h^5 f^{(4)}(k)) \tag{5.14}$$

$$\int_0^n p(t)dt \approx \sum_{k=1}^{\frac{n-1}{2}} \frac{h}{3}\left[v(2k-1) + 4v(2k) + v(2k+1)\right] + O(h^5 f^{(4)}(k)) \tag{5.15}$$

where $h = \Delta t$ is the sampling period, p is the position for a particular axis, and v and a are the linear velocity and linear acceleration respectively for that axis. The $O(h^5 f^{(4)}(k))$ term is a remainder term that is approximately 0 for small values of h.

The final step to computing the 3D position in the camera frame of reference is to add the initial position offset recorded during the calibration process described in Section 5.4.2:

$$\begin{bmatrix} x' \\ y' \\ z' \end{bmatrix} = \begin{bmatrix} x \\ y \\ z \end{bmatrix} + \begin{bmatrix} x_0 \\ y_0 \\ z_0 \end{bmatrix} \tag{5.16}$$

Chapter 6

Visual Tracking Unit (VTU)

This chapter describes in detail the overall design of the visual tracking unit (VTU). The first section presents an introduction to vision tracking systems. Section 6.2 provides a structural overview of the VTU. The object detection techniques used in the VTU are described in Section 6.3. Section 6.4 presents the techniques used to determine the position of the wireless 3D controller in the camera frame of reference. Finally, Section 6.5 present experimental results using the proposed VTU system.

6.1 Introduction

Visual tracking is the process of tracking one or more objects through the use of a optical device such as a camera system. Visual tracking has been used in a wide range of applications. These include: face tracking [SZM03], head tracking [MLCVA00, MJVR03], patient motion tracking [BGS+05], and augmented reality for medical procedures [VKS06]. Visual tracking systems can be divided into two gen-

eral groups. The first group are those that do not use markers for visual tracking. Such techniques rely on image registration and other complex computer vision techniques to track the motion of the desired object(s) and/or environment. Marker-less techniques are typically more computationally expensive. The second group of visual tracking systems are those that make use of distinctive markers placed on the object or environment being tracked. These techniques are typically less complex as markers are significantly easier to detect and track with greater accuracy. The visual tracking unit implemented in the proposed motion capture system is based on a marker tracking scheme where a marker placed at the front of the wireless 3D controller is tracked visually by a camera system.

The purpose and the overall design of the proposed motion capture system helps simplify the task of visually tracking the wireless 3D controller. First, the wireless 3D controller contains a single marker of uniform colour that needs to be tracked. As such, the object detection process can be simplified and the amount of processing required is effectively reduced. Second, the marker mounted on the wireless 3D controller for the purpose of tracking is a solid sphere. As such, its shape is invariant to rotation and thus reduce the complexity of the tracking system. Furthermore, the visual tracking system is used in conjunction with an inertial tracking system to eliminate the need for complex motion and orientation interpolation techniques. Finally, the purpose of the motion capture system is to allow for improved human-computer interactivity at close range to mid range distances. Therefore, the marker is close enough to the camera system that the size of the marker can be determined by the system. This size information is particularly useful for improving the position estimate.

6.2 VTU Structural Overview

The VTU used in the proposed motion capture system is implemented as part of the PC processing system. The general architecture of the VTU is illustrated in Figure 6.1. The architecture of the VTU is divided into two main components. The first component is responsible for detecting the actual marker embedded on the wireless 3D controller. The second component is responsible for determining the position of the detected marker in the camera frame of reference.

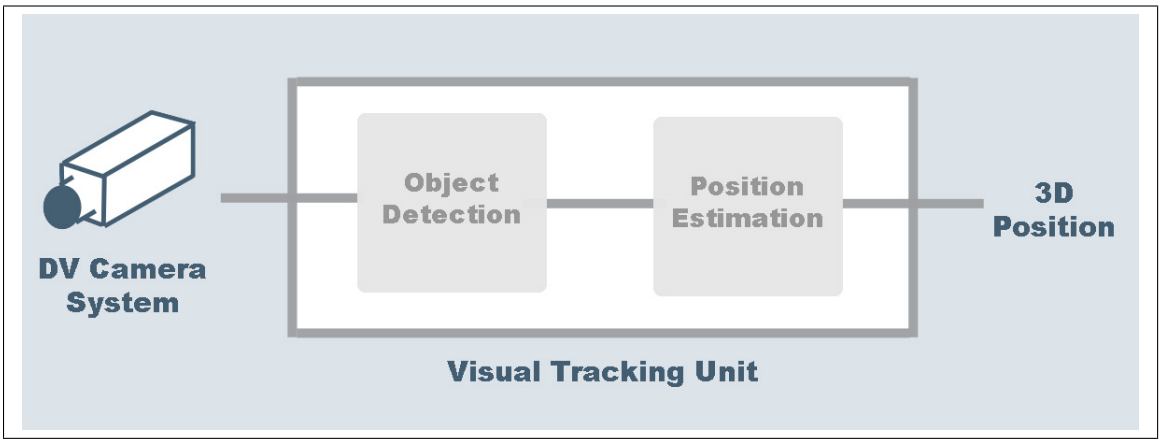

Figure 6.1: VTU setup

6.3 Object Detection

To perform visual tracking on the wireless 3D controller, it is necessary to detect the marker embedded at the front of the device from the visual data acquired by the camera system. Given that the physical characteristics of the marker are known, it is possible to devise an effective marker detection scheme based specifically on these characteristics. The object detection scheme used in the proposed motion

capture system is based on two important characteristics of the marker: i) colour, and ii) shape.

The first characteristic of the marker that is analysed by the object detection system is colour. Since the colour of the marker is uniform and known a priori, it is possible to reduce the search space and data in a particular video frame by first performing colour thresholding on the frame. There are a number of issues that must be considered before colour thresholding can be performed. The low-cost camera system used in the proposed motion capture system captures video content in the Red-Green-Blue (RGB) colour space. This colour space represents colour as a combination of additive primary colours. One issue associated with the RGB colour space with regards to its representation of colour is that the channels in the colour space are not easily separable.

The first issue related to this is that the RGB colour space is less intuitive for describing specific pure colours. This makes it more difficult to calibrate the system to detect the specific uniform colour ranges associated with the marker. The second and more important issue that needs to be dealt with is the problem of varying lighting conditions. Since the channels of the RGB colour space do not explicitly characterize illumination as an individual characteristic, the RGB value for an object under high illumination can be significantly different than if it was under low illumination as the colour and brightness of a pixel are coupled. One effective approach to addressing both these issues is to transform the colour information from the RGB colour space to the Hue-Saturation-Value (HSV) colour space. The HSV colour space represents colour as a combination of three components: i) Hue, ii) Saturation, and iii) Value. Hue represents a pure colour within the visible spectrum. Saturation represents the colour intensity of hue. The greater the saturation, the

more vivid and vibrant the hue appears. Finally, the value of the colour represents the overall brightness of the colour. A cylindrical visualization of the HSV colour space is illustrated in Figure 6.2.

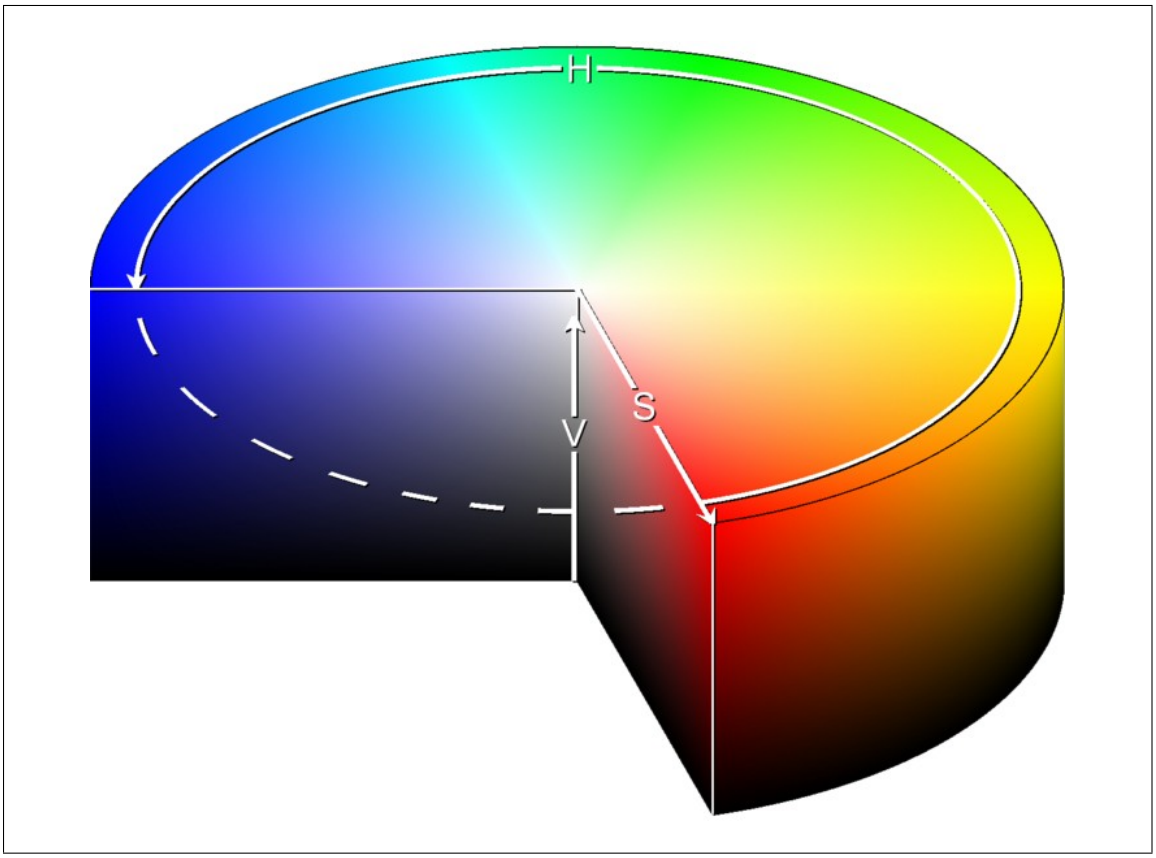

Figure 6.2: A cylindrical visualization of the HSV colour space [HSV06]

There are two main advantages to using the HSV colour space for the purpose of colour thresholding in the context of object detection when compared to the RGB colour space. First, the HSV colour space allows for a much more intuitive description of specific colours. This makes it easier to specify the colour threshold range of the marker using the hue and saturation channels as the colour of the marker is uniform and pure. The second benefit of using the HSV colour space is

that the hue and saturation of colour are decoupled from the brightness of colour. This allows for the colour threshold range of the marker to be specified independent of the brightness levels making colour detection robust to changes in illumination. In the proposed system, each video frame is converted from a RGB image into a HSV image as well as a greyscale image. If a particular pixel in the HSV image does not fall into the hue and saturation ranges specified for the target marker, the equivalent pixel in the greyscale image is set to 0. This effectively isolates the candidate pixels for the target marker in the greyscale image. The resulting threshold greyscale image is processed using an edge detector to produce a binary edge map of the scene. For the proposed system, the threshold image is first smoothed using a Gaussian kernel to reduce noise and then processed using a Sobel edge detector. The colour threshold and edge detection process is illustrated in Figure 6.3.

Once the binary edge map of the scene is computed, the second characteristic of the marker that is analysed is shape. Since the marker is in the shape of a sphere, it appears in the 2D image plane as a circle regardless of the view angle. Therefore, the marker can be detected as a circle in the binary edge map. One particularly robust and effective technique for circle detection is the Circular Hough Transform [DH72].

The Hough transform is a common method used to provide a global description of curve features in an image such as lines and circles. In the classical Hough transform, the points in a binary image as defined in the xy coordinate space are mapped into a coordinate space that is defined by the parameters of the curve feature being represented. For the case of line features, points in the xy coordinate space are mapped into a $\rho\theta$ parameter space, where ρ and θ correspond to the parameters of a line as defined by the line equation:

a) Original frame

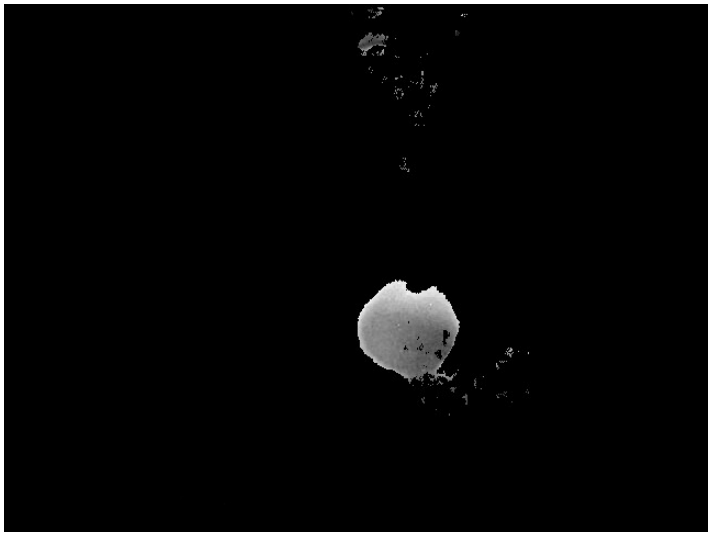

b) Initial threshold frame

Figure 6.3: Initial colour thresholding of video frame

$$xcos(\theta) + ysin(\theta) = \rho \tag{6.1}$$

where ρ represents the length of the normal vector going from the origin of the image (typically defined as the top-left corner of the image) to the line and θ represents the angular orientation of the normal vector with respect to the x-axis. In actual implementation, the $\rho\theta$ parameter space is discretized into what is referred as an accumulator array. Each point in the xy coordinate space corresponds to a curve in $\rho\theta$ parameter space, while each point in the $\rho\theta$ parameter space corresponds to a line in the xy coordinate space. An example illustrating an xy to $\rho\theta$ coordinate space mapping using the Hough transform is illustrated in Figure 6.4. Therefore, the value at location (ρ, θ) in the accumulator array represents the number of points in the binary image that lies on the line defined by the parameters rho and theta. Hence, line features can be recognized by detecting peaks in the accumulator array.

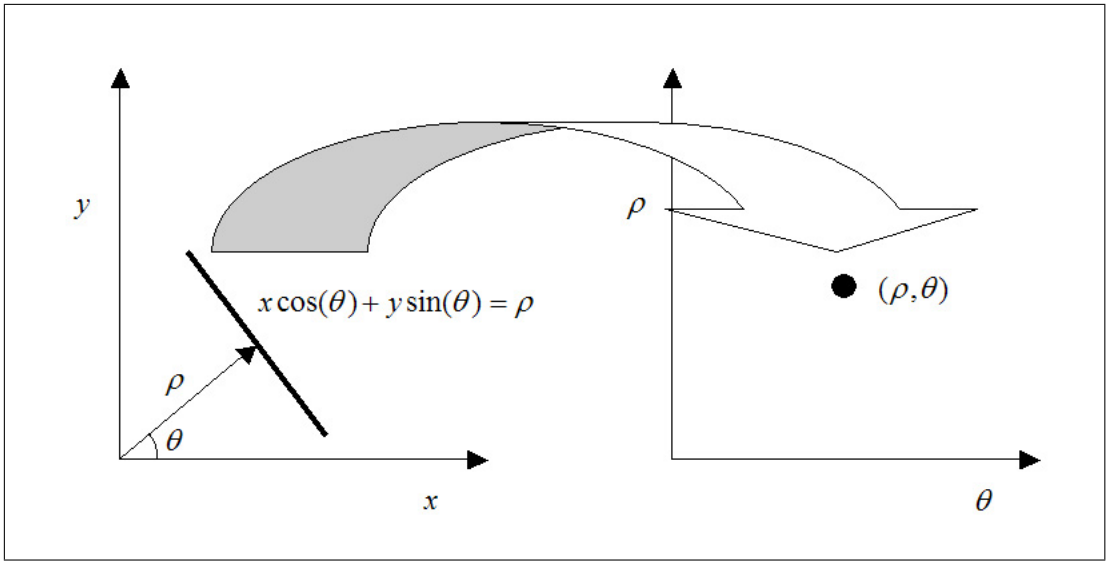

Figure 6.4: Classic Hough transform of a line

A similar approach to the classic Hough transform is taken for the Circular Hough Transform. Instead of the line equation, the parameters of a circle can be defined by the following circle equation:

$$(x - x_c)^2 + (y - y_c)^2 = r^2 \tag{6.2}$$

where x_c and y_c are the x and y coordinates of the center of the circle and r is the radius of the circle. This results in a 3D parameter space as defined by the parameters x_c, y_c, and r. For a fixed value of r, each point in the xy coordinate space of the image contributes to the center points (x_c, y_c) of a set of possible circles upon which the point lies on. This is illustrated in Figure 6.5. It can be clearly seen that a point in the xy coordinate space maps to a circle with the radius of r in the $x_c - y_c - r$ parameter space for that specific radius. By computing the parameter space for a range of radii, the parameters of the circle representing the marker is determined as the global maximum of the 3D parameter space. The main advantage of the Circular Hough Transform is that it is very robust against noise and discontinuities, making it well suited for non-ideal scenarios such as real-world environments.

While the search space was reduced using colour thresholding, the computation of Circular Hough Transform can still be computationally expensive as it needs to be computed for each radius. Therefore, a number of techniques were used to reduce the computational cost of performing the Circular Hough Transform process.

The first technique used was simply to reduce the range of radii that can be detected by the system. Since the purpose of the system is known, the range can be set according to the specific application. For example, if used for a home

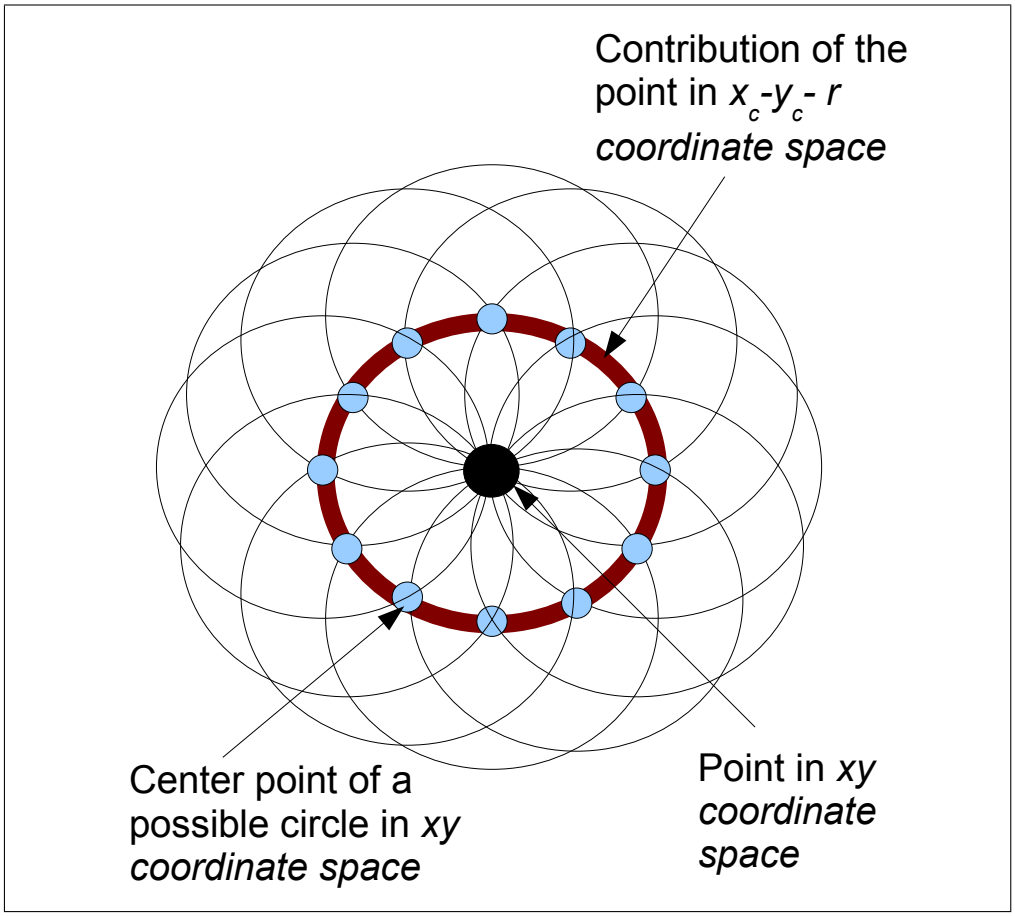

Figure 6.5: Circular Hough transform of a point

entertainment system such as a video game console, the wireless 3D controller is operated at a close range or mid range distance. Therefore, the range of the radii can be set such that it coincides with the radii of the marker as it appears in the image plane for that specific range of distances from the camera system.

The second technique used to reduce computational cost is based on the fact that a point in the xy coordinate space maps to a circle of a specific radius in the $x_c - y_c - r$ parameter space centered at $(x_c, y_c) = (x, y)$. Therefore, rather than calculate the contribution of the point in the parameter space using the standard circle equation, a more efficient approach is to plot the corresponding circle in the $x_c - y_c - r$ parameter space. This can be accomplished using a fast circle plotting algorithm such as the mid-point circle algorithm [Bre77]. The detection results for several video frames are shown in Figure 6.6. It can be seen that the object detection scheme performs well under different motions.

6.4 Position Estimation

Once the marker has been detected with respect to the 2D image plane, the 3D position of the marker in the 3D camera frame of reference needs to be determined. The position can be estimated using the center coordinates and radius of the marker in the image plane. Unlike professional motion capture systems, it is not feasible to calibrate the camera system by placing the marker at different predefined positions in a precise fashion. Therefore, it is necessary to make some generalizations and assumptions to simplify the model used for position estimation. First, it is assumed that the coordinates of the image plane have a linear mapping to that of the camera frame of reference. The second assumption is that the camera system is placed in

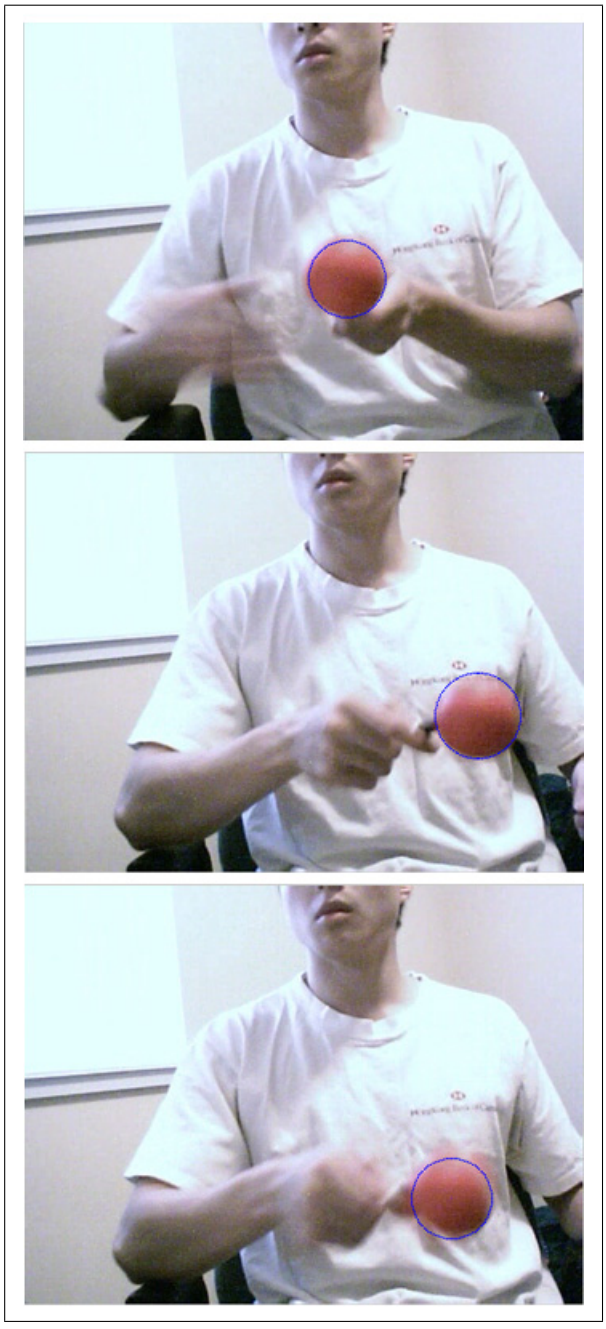

Figure 6.6: Results of object detection

a fixed location and will not be moved unless the calibration process is performed after the position change. Based on these assumptions, a suitable visualization model is the inverted pinhole camera model as illustrated in Figure 6.7.

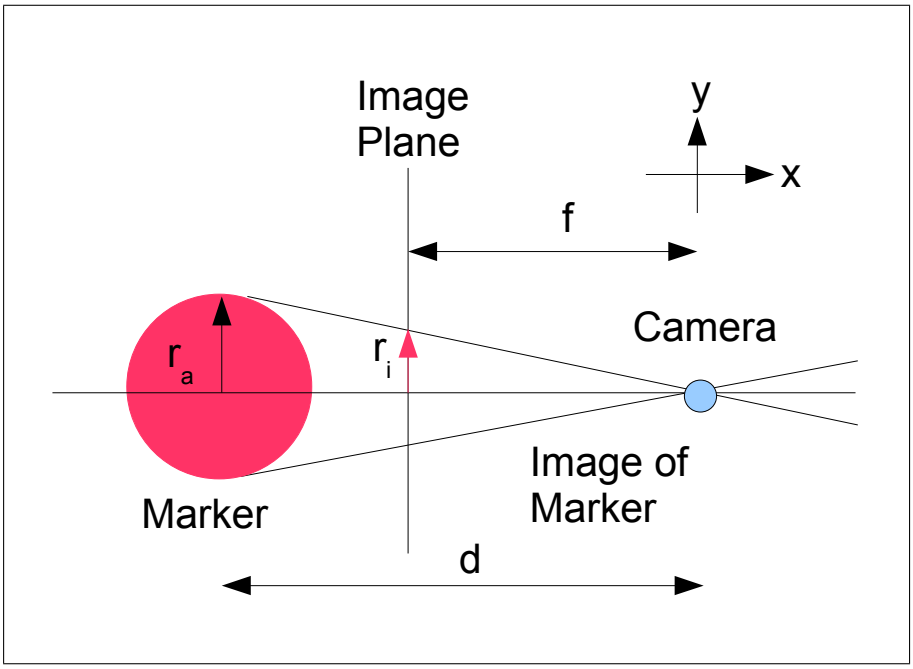

Figure 6.7: Inverted pinhole camera model

It can been seen that the radius of the marker in the image plane has a linear relationship with the radius of the actual marker in the camera frame of reference using this model. This relationship can be used to estimate the actual position of the marker along the image plane (which coincides with the yz plane) and the distance of the marker from the camera system (the x axis). As such, the image is defined by a yz coordinate system, where the origin is defined at the center of the image, where the z axis points to the top of the image and y axis points to the right of the image.

The position along the yz plane can be computed based on the radius of the

marker and that of the marker in the image plane using the following equation:

$$y_a = (r_a/r_{i,p})y_i \tag{6.3}$$

$$z_a = (r_a/r_{i,p})z_i \tag{6.4}$$

where (y_a, z_a) are the actual yz coordinates in the camera frame of reference, and (y_i, z_i) are the coordinates in the image plane, r_a is the actual radius of the marker, and $r_{i,p}$ is the radius of the marker in the image plane in pixels. The distance of the marker from the camera system can be computed using the following equation:

$$x_a = -d = -\frac{f}{r_i} r_a \tag{6.5}$$

where x_a is the x coordinate of the marker in the camera frame of reference, f is the focal length, r_a is the actual radius of the marker, and r_i is the radius of the marker in the image plane.

6.5 Experimental Results

To test the accuracy of the VTU, the marker was placed at different locations with known 3D coordinates. The estimated 3D position computed by the VTU was then compared to the reference 3D coordinates for each of the locations. A total of 10 test trials were conducted to analyse the overall 3D position estimation accuracy of the VTU. Furthermore, the tests were performed sequentially without system recalibration to observe the long-term stability of the system. Table 6.1 lists the specifications of the camera used for testing purposes.

Sensor Type	Focal Length	Video Resolution	Pixel Width	Frame Rate
CMOS	5 mm	640×480	6.0 μm	30 FPS

Table 6.1: Specifications of the test camera system

A summary of the position estimation accuracy results is shown in Table 6.2. It can be observed that the VTU is effective at estimating the 3D position of the marker. The RMS error is reasonably small and sufficient for the proposed system considering the low-end DV camera system being used for testing purposes. Therefore, it is evident that the VTU is capable of producing accurate results in long-term scenarios. This is particularly important for the purpose of complementing the INU system to produce 3D position information with improved accuracy and stability.

Test Type	RMS Error (cm)	Error Standard Deviation (cm)
y_a, z_a coordinates	0.1590	0.1210
x_a coordinates	0.5103	0.1516

Table 6.2: Summary of VTU position accuracy test

Chapter 7

Vision-Inertial Fusion Unit (VIFU)

This chapter describes in detail the overall design of the vision-inertial fusion unit (VIFU). The first section presents an introduction to sensor data fusion. The underlying theory behind two different sensor fusion techniques (complementary filters and Kalman filters) are described in Section 7.2. Section 7.3 provides a structural overview of the VIFU. Finally, Section 7.4 presents the error model used in the error-state complementary Kalman filter of the VIFU.

7.1 Introduction

Sensor data fusion is the process of combining sensory data from multiple, different sensor acquisition sources. The sensor sources can be composed of homogeneous sensors (i.e., a sensor network of cameras) or heterogeneous sensors (i.e., cameras

coupled with accelerometers). There are a number of different reasons for performing sensor data fusion.

First, sensor data fusion may be performed to produce information that is more accurate and detailed than possible using a single sensor device. For example, sensor readings from a highly accurate but low frequency sensor can be combined with sensor readings from a less accurate but high frequency sensor to produce accurate and detailed sensor readings.

Another reason for sensor data fusion is to produce information that provides a more complete picture of the environment than can be obtained a single sensor. For example, multiple sensors can placed to observe non-overlapping regions spatially or temporally to acquire different sensor readings on a particular scene. One practical application of this approach is image super-resolution where data acquired by multiple cameras placed at different positions is combined to produce an image at a higher resolution than that of any individual camera. Finally, sensor data fusion may be performed to improve the robustness of the system against individual sensor failures. This is useful in scenarios where one or more sensors in a sensor network may fail due to environmental or technical circumstances. One practical application for this approach is wide area environment monitoring, where many low-cost sensors are deployed to ensure adequate sensor readings. This is particularly important in hazardous environments where sensors are prone to failure.

Sensor fusion may be divided into three general classes [Kov01]: i) complementary, ii) cooperative, and iii) competitive. In complementary sensor fusion, individual sensors either acquire sensor readings on different (adjacent) environments or contribute sensor readings on different aspects of the same environment. Sensor readings acquired by individual sensors for the purpose of complementary

sensor fusion often have little or no overlap and can be combined to create a more complete picture of the environment. In general, complementary sensor fusion does not yield new information that cannot be measured directly by one or more of the individual sensors.

In cooperative sensor fusion, sensor data from individual sensors are used to produce new information that cannot be measured directly by an individual sensor. An example of this is stereoscopic sensor fusion which takes 2D images acquired by cameras at different viewpoints to produce a 3D representation of the environment. The 3D information cannot be measured directly by any one of the individual cameras.

Finally, competitive sensor fusion makes use of equivalent information about the environment from individual sensors. This is typically used to provide redundancy in case of individual sensor device failures. This technique can also be used to improve the reliability of the sensor results.

The VIFU in the proposed system is a complementary sensor fusion system that combines data obtained from heterogenous sensors (inertial and visual sensors). While the accelerometer sensors can acquire information at a very high sampling rate to produce a very detailed picture of the motion of the wireless 3D controller, they are unable to maintain long-term accuracy due to rapid error accumulation. On the other hand, the visual sensor system is capable of maintaining long-term accuracy but can only acquire information at a low sampling rate due to technical and computational limitations. Therefore, the VIFU exploits the advantages of each of these sensor types to produce 3D position data that provides greater detail than that possible with the visual sensor system and greater long-term stability than can be achieved using only the inertial sensor system.

7.2 Sensor Fusion Techniques

The first step to designing the VIFU for the proposed system is to determine the sensory fusion technique to be used. Two of the most widely used techniques for sensor fusion are: i) complementary filters, and ii) Kalman filters.

7.2.1 Complementary Filters

There are many situations where sensors with different noise and frequency characteristics are used to to measure the same physical phenomenon at the same time. It is often the case by design that one sensor source provides higher sensitivity and/or less noise at one frequency band while another sensor source provides higher sensitivty and/or less noise at another frequency band. For example, a camera sensor device provides better sensory data at low frequencies while an inertial sensor device provides better data at high frequencies. Therefore, it is desirable to combine the low frequency characteristics of the camera system and the high frequency characteristics of the inertial sensor.

This can be achieved through the use of a complementary filter system. A complementary filter system is a pair of filters whose transfer functions add up to one at all frequencies [WHL04]. A typical complementary filter system is composed of a low pass filter, a high pass filter, and a combiner. In the case of a heterogenous sensor system consisting of a visual sensor system and an inertial sensor system, the data from the visual sensor system is filtered by a low-pass filter and the data from the inertial sensor system is filtered by a high-pass filter. The two filtered data signals are then summed up by the combiner to produce a final output signal. This process is illustrated in Figure 7.1. One of the main advantages of a complementary

filter system is that it is relatively simple to implement. However, it does not take into account error sources such as bias errors.

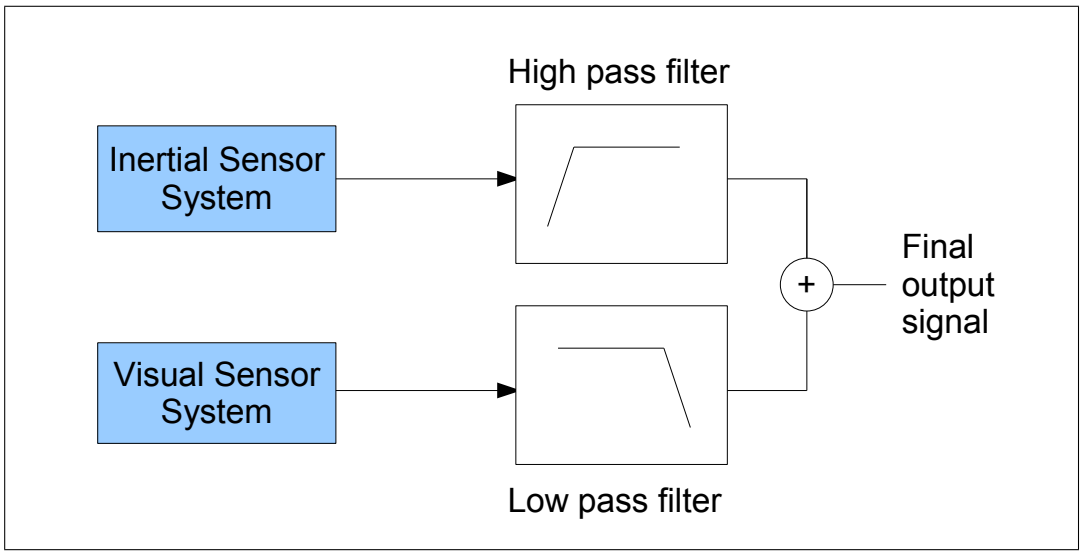

Figure 7.1: Complementary filter system

7.2.2 Kalman Filters

Another widely used technique for sensor fusion is the use of a Kalman filter [Kal60]. The Kalman filter is a recursive discrete data filter is used to perform state estimation for dynamic systems. Kalman filters have been used extensively in a wide range of fields, particularly in the area of navigation and control systems. These filters are popular for a number of reasons. First, they are computationally efficient. Second, they are very versatile and capable of providing good state estimates for past time, present time, and future time. Finally, they are able to use dynamic models and error models of the underlying system to effectively reduce the effects of noise on the resulting state estimates. Therefore, a Kalman filter approach is

better suited than the complementary filter approach in situations where the sensor data may be corrupted by noise.

Rather than explaining in detail the mathematical theory of Kalman filters, the general implementation methodology is presented in context of inertial navigation systems. The discrete Kalman filter can be seen as a series of equations that take a state estimate from the previous time step and a measurement from the current time step to determine an estimate of the current state of the dynamic system. The Kalman filter makes use of a dynamic model and an observation model of the system. The dynamic model can be generalized as follows (neglecting optional control inputs):

$$x_k = \mathbf{A}x_{k-1} + w_{k-1} \tag{7.1}$$

where x is the state of the system, k is the current time step, the matrix $\mathbf{A}$ is the dynamic model that relates the state at the previous time step to that at the current time step, and w represents the process noise. The observation model can be generalized as:

$$z_k = \mathbf{H}x_k + v_k \tag{7.2}$$

where z is the measurement at a specific time step, $\mathbf{H}$ is the observation model that relates the state of the system with the measurement, and v represents the measurement noise. The measurement noise and the process noise are assumed to be zero-mean, white, and normally distributed:

$$p(w) \sim N(0, Q) \tag{7.3}$$

$$p(v) \sim N(0, R) \tag{7.4}$$

where Q and R are the process noise covariance and the measurement noise covariance respectively. In the case of inertial data, the dynamic model consists of a system of dynamic equations used to compute position/orientation, velocity, and acceleration.

The Kalman filter is divided into a prediction step and an update step. The first step is the prediction step which predicts the state at the current time step based on an estimate of the previous time step. The prediction step is defined by the following equations (neglecting optional control inputs):

$$\hat{x}_{k|k-1} = \mathbf{A}\hat{x}_{k-1|k-1} \tag{7.5}$$

$$\mathbf{P}_{k|k-1} = \mathbf{A}\mathbf{P}_{k-1|k-1}\mathbf{A}_k^T + \mathbf{Q}_k \tag{7.6}$$

where $\hat{x}_{k|k-1}$ is an estimate at time step k using only knowledge about the process at the previous time step, and $\mathbf{P}_{k|k-1}$ is the error covariance at time step k using knowledge about the process at the previous time step.

The second step of the Kalman filter process is the update step, which adjusts the state estimate made in the prediction step using the measurement made at the current time step such that mean squared error is minimized:

$$\mathbf{K}_k = \mathbf{P}_{k|k-1}\mathbf{H}^T(\mathbf{H}\mathbf{P}_{k|k-1}\mathbf{H}^T + \mathbf{R})^{-1} \tag{7.7}$$

$$\hat{x}_k = \hat{x}_{k|k-1} + \mathbf{K}_k(z_k - \mathbf{H}\hat{x}_{k|k-1}) \tag{7.8}$$

$$\mathbf{P}_k = (\mathbf{I} - \mathbf{K}_k\mathbf{H})\mathbf{P}_{k|k-1} \tag{7.9}$$

where $\mathbf{K}$ is the Kalman gain and $\mathbf{I}$ is the identity matrix. After the state and error covariance has been estimated for the current time step, this can then be used to make subsequent estimates at other time steps. A Kalman filter based approach is used in the proposed system because of its ability to handle noisy sensor data. This is particularly important for the inertial sensors used in the proposed system since these sensors provide measurements that can be corrupted by various types of measurement noise.

7.3 VIFU Structural Overview

The VIFU used in the proposed motion capture system is implemented as part of the PC processing system. The general architecture of the VIFU is illustrated in Figure 7.2. The 3D position information from the VTU and the INU are fed into an error-state complementary Kalman filter system which fuses the sensor data from both sources into a unified 3D position data output.

7.4 Error-State Complementary Kalman Filter

The VIFU is laid out into what is known as an error-state complementary Kalman filter configuration [May79, CDW94]. This is illustrated in Figure 7.3. In this configuration, the difference is calculated between the 3D position output from the INU and from the VTU. Using the output of the VTU as the reference point, the

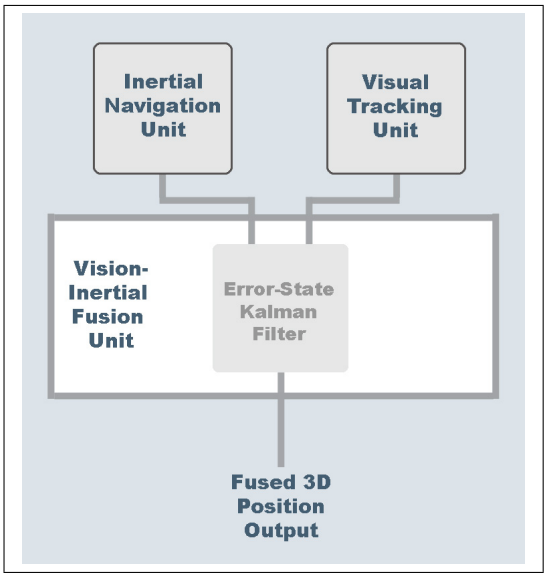

Figure 7.2: VIFU setup

difference represents the position error of the INU. This position error signal is then used as the measurement signal to the Kalman Filter. In an error-state Kalman complementary filter configuration, the classic Kalman filter is used to continually estimate the error of the inertial sensor data. The error estimates are then used to correct the inertial sensor data outputs of the INU. The advantage of using an error-state complementary Kalman filter configuration is that the detailed information from the INU data at high frequencies can be preserved while the errors in the low frequencies can be corrected. This results in an output signal that is detailed and maintains long-term reliability.

Since the Kalman filter is used to provide an error estimate for the inertial sensor data from the INU, it is necessary to establish an error model and observation model for the system. Since the constant bias error in the inertial sensor data has been corrected in the INU, the primary goal of the error-state complementary Kalman

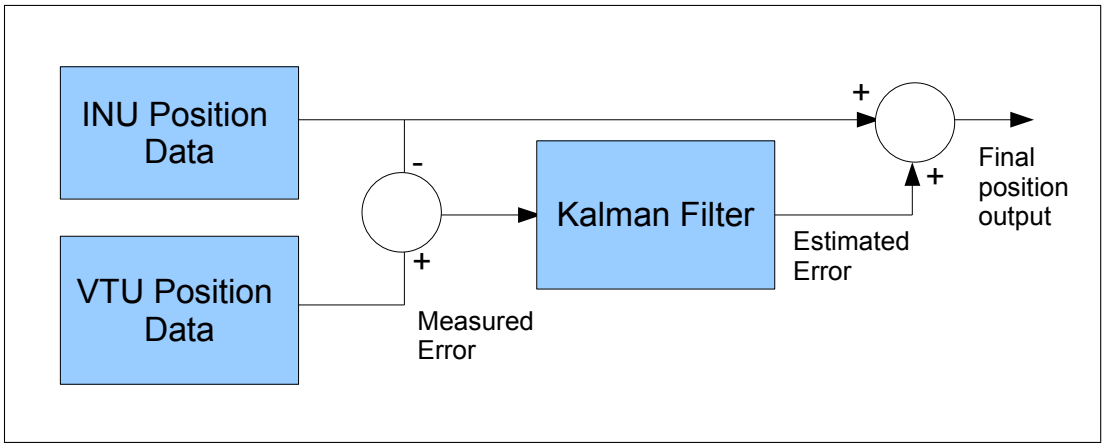

Figure 7.3: Error-state complementary Kalman filter

filter system is to correct the time-varying error bias discussed in Section 4.4. The error model used in the proposed system can be defined using the following set of linear difference equations:

$$e_p[k] = e_p[k-1] + e_v[k-1]\Delta t + \frac{1}{2}e_a[k-1]\Delta t^2 \tag{7.10}$$

$$e_v[k] = e_v[k-1] + e_a[k-1]\Delta t \tag{7.11}$$

$$e_a[k] = e_a[k] + w_{k-1} \tag{7.12}$$

where e_p, e_v, and e_a are the errors for position, velocity, and acceleration respectively, k is the current time, Δt is the time step, and w represents the process noise. Since the position error signal is used as the measurement signal to the Kalman Filter, the error observation model is defined by the following equation:

$$z[k] = e_p[k] + v_k \tag{7.13}$$

where z is the measured position error at a specific time step and v represents the measurement noise.

Based on the above error model and observation model, the Kalman filter state space matrices are given by:

$$\mathbf{A} = \begin{bmatrix} 1 & \Delta t & \frac{1}{2}\Delta t^2 \\ 0 & 1 & \Delta t \\ 0 & 0 & 1 \end{bmatrix} \tag{7.14}$$

$$\mathbf{H}_{\mathrm{VTU_{On}}} = \begin{bmatrix} 1 & 0 & 0 \end{bmatrix} \tag{7.15}$$

$$\mathbf{H}_{\mathrm{VTU_{Off}}} = \begin{bmatrix} 0 & 0 & 0 \end{bmatrix} \tag{7.16}$$

$$\mathbf{Q} = \begin{bmatrix} \sigma^2_{\mathrm{pnoise}} & 0 & 0 \\ 0 & \sigma^2_{\mathrm{pnoise}} & 0 \\ 0 & 0 & \sigma^2_{\mathrm{pnoise}} \end{bmatrix} \tag{7.17}$$

$$\mathbf{R} = \begin{bmatrix} \sigma^2_{\mathrm{mnoise}} \end{bmatrix} \tag{7.18}$$

where $\mathbf{H}_{\mathrm{VTU_{On}}}$ is the observation model matrix when data is available from the VTU, $\mathbf{H}_{\mathrm{VTU_{Off}}}$ is the observation model matrix when data is not available from the VTU, $\sigma^2_{\mathrm{pnoise}}$ is the process noise variance and $\sigma^2_{\mathrm{mnoise}}$ is the measurement noise variance.

To test the effectiveness of the error-state complementary Kalman filter, the

position accuracy tests introduced in Chapter 4 were performed on the enhanced system. For the purpose of the tests, the wireless 3D controller was left in a fixed location with no external forces being exerted on the device. The VTU was configured such that position information was available to the VIFU at a sampling rate of 2 samples/second. This enabled an investigation of the effectiveness of the system with visual data available at a very low frequency. Such a scenario is common for consumer-level devices and applications. The results of the position accuracy tests are presented in Table 7.1.

Test No.	**Original Results**		**Filtered Results**	
	Mean Accumulated Error (m)	**Error Standard Deviation (m)**	**Mean Accumulated Error (m)**	**Error Standard Deviation (m)**
1	0.156	0.0112	0.00287	0.0017
2	1.540	0.1784	0.00355	0.0018
3	2.6885	0.4014	0.00383	0.0025
4	8.0794	0.7622	0.01087	0.0020

Table 7.1: Summary of position accuracy tests

A graph illustrating the position error for the x channel for a time period of 63.96 s with and without the error-state complementary Kalman filter is shown in Figure 7.4. It can be observed that filtering significantly reduces the position error. Furthermore, the position error after filtering remains consistent and stable over the entire measurement time period. Therefore, it is evident that the error-state complementary Kalman filter can be used effectively to fuse information from the VTU and the INU into a 3D position output that is both detailed and reliable over time.

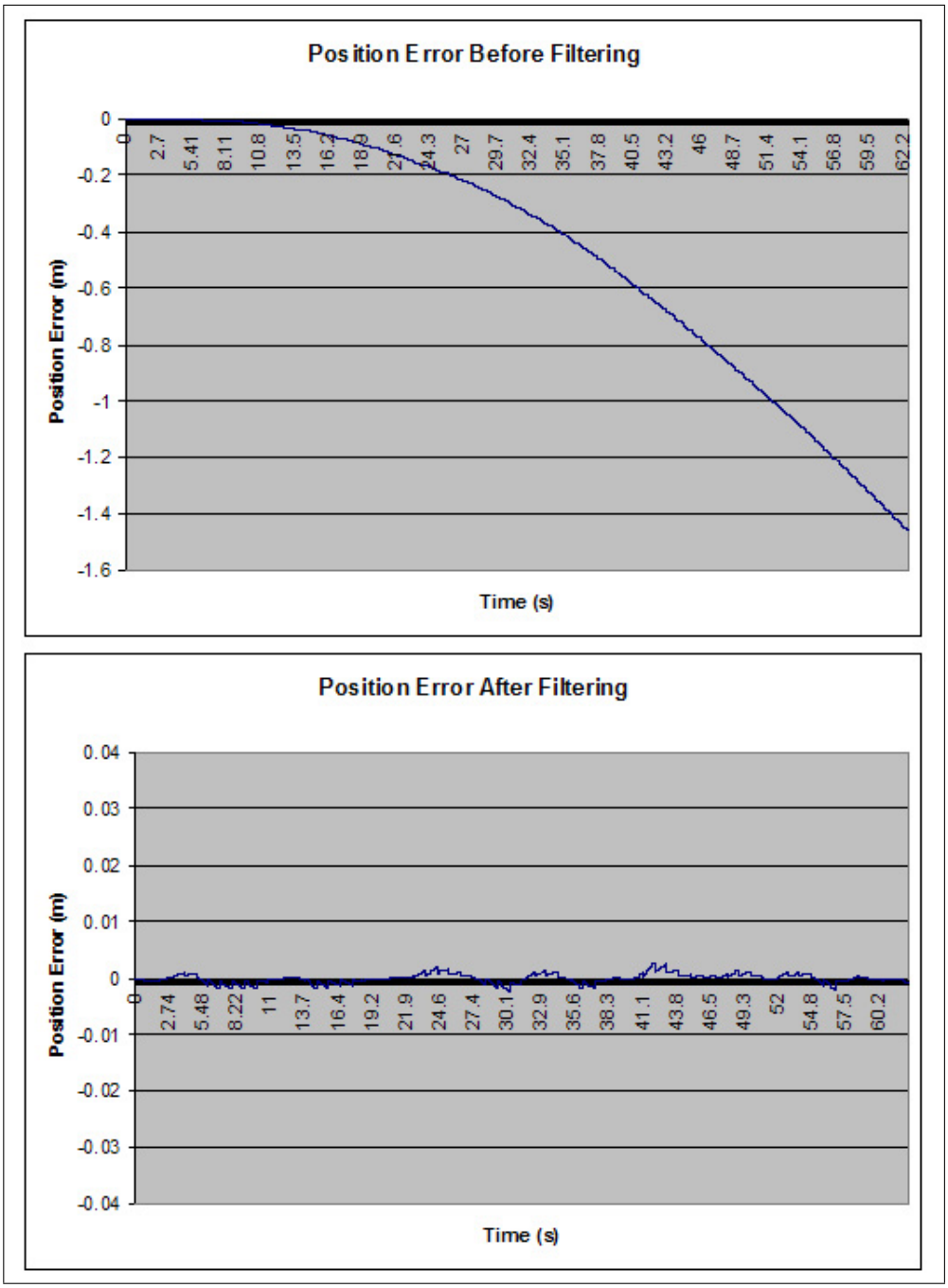

Figure 7.4: Position error over time for error-state complementary Kalman filter

Chapter 8

Conclusions

A vision-inertial motion capture system for wireless 3D controllers is capable of providing detailed and reliable 3D position and orientation information using only low-cost inertial sensors and visual sensors. Inertial tracking systems using accelerometers and gyro sensors provide accurate high frequency motion readings but suffer from rapid error accumulation. Visual tracking systems using one or more cameras provide accurate motion readings at low frequencies but high frequency motion readings are not possible due to the relatively high processing demands of object detection. By transforming the inertial data to coincide with the visual data, the sensor data from the two types of sensors can be fused to provide better 3D position readings than otherwise possible using either a visual tracking system or an inertial tracking system alone.

8.1 Thesis Contributions

The thesis dissertation presents a design study on a visual-inertial motion capture system for wireless 3D controllers. The results of this study demonstrate the feasibility of such a device for consumer-level applications. This thesis provides a foundation for future research in consumer-level hybrid motion capture systems for human computer interfaces by making several contributions. The primary contributions of the dissertation include:

- describes the design of a visual-inertial hybrid motion capture system using low-cost sensor components,
- provides experimental results demonstrating the error accumulation of inertial devices when used to derive 3D position information,
- describes calibration methods for synchronizing inertial sensor data with visual sensor data,
- provides experimental results demonstrating the effectiveness of combining colour thresholding, a circular Hough transform, and distance measurement using a pinhole camera model to visually track an object in 3D space in a computationally efficient manner, and
- provides experimental results demonstrating the effectiveness of the error-state complementary Kalman filter in producing better 3D position by fusing visual sensor data with inertial sensor data.

The secondary contributions of the dissertation include:

- introduces and explains the concepts associated with the design of motion capture systems, and
- presents several of the challenges associated with the design of a low-cost hybrid motion capture system.

8.2 Potential for Future Research

The research presented in this dissertation provides a foundation for future research in consumer-level hybrid motion capture systems. Two potential research topics that can build upon the research presented in this dissertation are the following:

- low-cost multi-marker visual-inertial motion capture systems, and
- mainstream software applications utilizing motion capture.

8.2.1 Low-Cost Multi-Marker Visual-Inertial Motion Capture

For the purpose of this research, a motion capture system was designed for tracking a single wireless 3D controller. As the device has no moveable parts, a single marker was tracked by the proposed system. Future research could expand the system to track multiple markers placed on a device with moveable parts and/or a user's body while still utilizing low-cost sensor devices. This research could lead to a number of different consumer-level applications such as low-cost motion capture systems for small animation studios and consumer-level interactive video games where virtual

objects are manipulated in real-time using hand motion. An investigation of the feasibility of building such a device using low-cost components is recommended.

8.2.2 Mainstream Software Applications Utilizing Motion Capture

The objective of the research presented in this thesis is the design of the actual motion capture system used to track a wireless 3D controller. However, such a system would not be useful without mainstream software applications that can utilize it to its full potential. Current mainstream software applications that can make use of the proposed system include writing and drawing tools as well as 3D modeling tools. However, these applications are not designed around such a system and therefore do not take full advantage of the level of freedom and interactivity the proposed system can deliver. Therefore, an investigation into possible future mainstream software applications that can truly take advantage of the proposed system is recommended.

8.3 Thesis Applicability

The work presented in this thesis has provided a practical solution to motion capture using wireless 3D controllers. Experimental results show that it is possible to implement the proposed system using low-cost visual and inertial sensor devices. Therefore, the proposed system is well-suited for consumer-level applications that can utilize motion-based input from a user, such as virtual reality systems, video games, and motion capture for character animation.

Bibliography

[ADBW02] J. Gorman A. Duwel, M. Weinstein, J. Borenstein, and P. Ward. Quality factors of MEMS gyros and the role of thermoelastic damping. In *Proceedings of The Fifteenth IEEE International Conference on Micro Electro Mechanical Systems*, pages 214–219, 2002.

[Ani06] Gypsy5 Mechanical Motion Capture. World Wide Web Document, October 2006. `http://www.animazoo.com/products/gypsy5.htm`.

[Asc06] MotionStar. World Wide Web Document, October 2006. `http://www.ascension-tech.com/products/motionstar.php`.

[BGS+05] P. Bruyant, M. Gennert, G. Speckert, R. Beach, J. Morgenstern, N. Kumar, S. Nadella, and M. King. A Robust Visual Tracking System for patient motion. *IEEE Transaction on Nuclear Science*, 52(5):1288–1294, October 2005.

[Blo06] J. Blomster. Orientation estimation combining vision and gyro measurements. Master's thesis, Royal Institute of Technology, April 2006.

[Boy05] J. Boyd. Good Vibrations from Epsons New Gyro-Sensor. *Technology Newsline*, 12, February 2005.

[Bre77] J. Bresenham. A linear algorithm for incremental digital display of circular arcs. *Communications of the ACM*, 20(2):100–106, 1977.

[CDW94] S. Cooper and H. Durrant Whyte. A frequency response method for multi-sensor high-speed navigation systems. In *Proceedings of IEEE International Conference on Multisensor Fusion and Integration for Intelligent Systems*, pages 1–8, October 1994.

[CJD03] Y. Caritu C. Joguet and D. David. 'Pen-like' natural graphic gesture capture disposal, based on a micro-system. In *Smart Objects Conference*, May 2003.

[DGEE03] J. Powell D. Gebre Egziabher, C. Lee Boyce Jr. and P. Enge. An Inexpensive DME-Aided Dead Reckoning Navigator. *Navigation*, 50(4):247–264, Winter 2003.

[DH72] R. Duda and P. Hart. Use of the Hough Transform to detect lines and curves in pictures. *Communications of the ACM archive*, 15(1):11–15, January 1972.

[EFGP98] M. Harrington E. Foxlin and George Pfeifer. Constellation: A wide-range wireless motion-tracking system for augmented reality and virtual set application. In *Proceedings of SIGGRAPH 98*, pages 371–378, 1998.

[Eye06] Eyetoy. World Wide Web Document, October 2006. `http://www.eyetoy.com`.

[FN03a] E. Foxlin and L. Naimark. Miniaturization, calibration & accuracy evaluation of a hybrid self-tracker. In *Proceedings of the 2nd IEEE and ACM International Symposium on Mixed and Augmented Reality*, pages 151–160, Washington, DC, USA, 2003. IEEE Computer Society.

[FN03b] E. Foxlin and L. Naimark. Vis-tracker: A wearable vision-inertial self-tracker. In *Proceedings of IEEE Virtual Reality*, pages 199–206, March 2003.

[GE04] D. Gebre Egziabher. *Design and Performance Analysis of A Low-cost Aided Dead Reckoning Navigator*. PhD thesis, Stanford University, February 2004.

[HSV06] HSV color space. World Wide Web Document, October 2006. `http://en.wikipedia.org/wiki/HSV_color_space`.

[Int07] InterSense Wireless InertiaCube3. World Wide Web Document, March 2007. `http://www.isense.com/uploadedFiles/Products/WirelessInertiaCube3.pdf`.

[JLA95] J. Dias J. Lobo, P. Lucas and A. Almeida. Inertial Navigation System for Mobile Land Vehicles. In *Proceedings of ISIE95*, pages 843–848, 1995.

[JOH00] G. Brostow J. O'Brien, B. Bodenheimer and J. Hodgins. Automatic Joint Parameter Estimation from Magnetic Motion Capture Data. In *Proceedings of Graphics Interface 2000*, pages 53–60, May 2000.

[Kal60] R. Kalman. A New Approach to Linear filtering and prediction problems. *Transaction of the ASME-Journal of Basic Engineering*, pages 35–45, March 1960.

[KD04] G. Klein and T. Drummond. Tightly integrated sensor fusion for robust visual tracking. *Image and Vision Computing*, 22(10):769–776, September 2004.

[KGK02] J. Junkins K. Gunnam, D. Hughes and N. Kehtornavaz. A DSP embedded optical navigation system. In *Proceedings of the 6th International Conference on Signal Processing*, volume 2, pages 1735–1739, 2002.

[Kio06] Kionix. World Wide Web Document, October 2006. `http://www.kionix.com/`.

[Kov01] V. Koval. The competitive sensor fusion algorithm for multi sensor systems. In *International Workshop on Intelligent Data Acquisition and Advanced Computing Systems: Technology and Applications*, pages 65–68, July 2001.

[Lui02] H. Luinge. *Inertial Sensing of Human Movement*. PhD Dissertation, University of Twente, December 2002.

[May79] P. Maybeck. *Stochastic Models, Estimation and Control*, volume I. Academic Press, New York, 1979.

[Mic07] G-Link 2.4 GHz Wireless Accelerometer Product Datasheet. World Wide Web Document, March 2007. `http://www.microstrain.com/product_datasheets/2400_g-link_datasheet.pdf`.

[MJVR03] J. Mulder, J. Jansen, and A. Van Rhijn. An affordable optical head tracking system for desktop vr/ar systems. In *Proceedings of the workshop on Virtual environments 2003*, pages 215–223, 2003.

[MLCVA00] S. Sclaroff M. La Cascia and Vassilis Athitsos. Fast, reliable head tracking under varying illumination: An approach based on registration of texture-mapped 3d models. *IEEE Transaction on Pattern Analysis and Machine Intelligence*, pages 322–336, April 2000.

[NDI06] NDI. World Wide Web Document, October 2006. `http://www.ndigital.com/`.

[Pha06] Phasespace. World Wide Web Document, October 2006. `http://www.phasespace.com/`.

[RLG+02] M. Ribo, P. Lang, H. Ganster, M. Brandner, C. Stock, and A. Pinz. Hybrid tracking for outdoor augmented reality applications. *IEEE Computer Graphics and Applications*, 22(6):54–63, November/December 2002.

[Roe06] D. Roetenberg. *Inertial and Magnetic Sensing of Human Motion*. PhD Dissertation, University of Twente, May 2006.

[Sch06] A. Schumacher. Integration of a gps aided strapdown inertial navigation system for land vehicles. Master's Thesis, Royal Institute of Technology, March 2006.

[SH05] I. Skog and P. Handel. A Low-cost gps aided inertial navigation system for vehicle applications. In *Proceedings of the Thirdteenth European Signal Processing Conference*, September 2005.

[SYA99] U. Neumann S. You and R. Azuma. Hybrid inertial and vision tracking for augmented reality registration. In *Proceedings of IEEE Virtual Reality*, pages 260–267, March 1999.

[SZM03] R. Chellappa S. Zhou and B. Moghaddam. Adaptive Visual Tracking and Recognition using Particle Filters. In *Proceedings of IEEE International Conference on Multimedia and Expo*, pages 349–352, July 2003.

[Vic06] Vicon. World Wide Web Document, October 2006. `http://www.vicon.com`.

[VKS06] S. Vogtl, A. Khamenel, and F. Saueri. Reality augmentation for medical procedures: System architecture, single camera marker tracking, and system evaluation. *International Journal of Computer Vision*, 70(2):179–190, November 2006.

[WHL04] C. Hardham W. Hua, D. DeBra and B. Lantz. Polyphase FIR complementary filters for control systems. In *Proceedings of Spring Topical Meeting on Control of Precision Systems*, pages 109–114, April 2004.

[Wii06] Wii. World Wide Web Document, October 2006. `http://www.wii.com`.

[YAG+03] S. Yu, C. Allen, D. Geng, D. Burn, U. Brechany, G. Bell, and R. Rowland. 3-D motion system (data-gloves): application for parkinson's disease. *IEEE Transactions on Instrumentation and Measurement*, 52(3):662–674, June 2003.